

INHIBITION OF MITOGEN-ACTIVATED PROTEIN KINASE  
P38 $\alpha$  BY ROOPEROL AND ANALOGUES

by

Chelsea Savannah Davis, B.S.A

A thesis submitted to the Graduate Council of  
Texas State University in partial fulfillment  
of the requirements for the degree of  
Master of Science  
with a Major in Biochemistry  
August 2020

Committee Members:

Sean M. Kerwin, Chair

Karen A. Lewis

L. Kevin Lewis

**COPYRIGHT**

by

Chelsea Savannah Davis

2020

## **FAIR USE AND AUTHOR'S PERMISSION STATEMENT**

### **Fair Use**

This work is protected by the Copyright Laws of the United States (Public Law 94-553, section 107). Consistent with fair use as defined in the Copyright Laws, brief quotations from this material are allowed with proper acknowledgement. Use of this material for financial gain without the author's express written permission is not allowed.

### **Duplication Permission**

As the copyright holder of this work I, Chelsea Savannah Davis, authorize duplication of this work, in whole or in part, for educational or scholarly purposes only.

## **DEDICATION**

“People don’t *care* how much you *know*, until they *know* how much you *care*.”

-Theodore Roosevelt

This achievement is dedicated to the village who have made sure that as my knowledge increases that my kindness for others increases, becoming a better equipped & more compassionate version of myself. To my parents, Jeanne & Brad, my brother, Happy, to my Aunties and Uncles, Granny and Grandad, whose love knows no bounds. To my dearest Katie, Nathan, Victoria, Iliana, and Jennifer who each provided loyal, kind, loving, authentic support over this wild season and encouraged me up to reach this great mountain top.

## **ACKNOWLEDGEMENTS**

With sincerest gratitude I thank my research advisor Dr. Sean M. Kerwin, who with great patience, finesse, and kindness supported me in the work produced herein. I would also like to thank my committee members Dr. L. Kevin Lewis and Dr. Karen Lewis, for their efforts towards my improvement both in and outside of the classroom, with their expertise, guidance, and invaluable point of view. I would like to thank the members of the Kerwin Lab for being a sounding board for all things rooperol and G-quadruplex, as well as creating an environment of learning and support. I would like to express my sincerest gratitude to Kate Banks, Amanda Bohannon, Brandie Taylor, and Samantha Zepeda who all welcomed, supported, mentored, and gave a many a needed push for success in lab and in my master's studies.

## TABLE OF CONTENTS

	<b>Page</b>
ACKNOWLEDGEMENTS .....	v
LIST OF TABLES .....	vii
LIST OF FIGURES .....	viii
LIST OF ABBREVIATIONS .....	x
ABSTRACT .....	xi
CHAPTER	
I. BACKGROUND .....	1
II. EXPERIMENTAL .....	10
III. RESULTS AND DISCUSSION .....	17
IV. CONCLUSION .....	43
APPENDIX SECTION .....	45
LITERATURE CITED .....	60

## LIST OF TABLES

<b>Table</b>	<b>Page</b>
1. Volumes of ATP and ADP for Percentage Conversion Curve .....	14
2. Predicted binding affinities of rooperol and analogues docked onto 1LEW .....	36
3. Cytotoxicity and highest predicted affinity data of tested rooperol and analogues.....	40

## LIST OF FIGURES

Figure	Page
1. African Potato and Conversion of Hypoxoside to Rooperol .....	3
2. MAPK Pathway .....	5
3. Docking Sites on p38 $\alpha$ .....	6
4. DRS/KIM Binding Site.....	7
5. Rooperol Analogue Overview .....	8
6. Signal to Noise Optimization ATF2 Concentration.....	18
7. Signal to Noise Optimization Phosphatase Incubation.....	19
8. Signal to Noise Optimization Goettert Protocol .....	20
9. Kinase Dependence ELISA .....	21
10. ADP Conversion Curve with ADP-Glo™ Assay .....	23
11. Hexokinase Enzyme Curve and ADP Conversion Curve.....	25
12. Initial Rooperol Docking Results.....	27
13. DRS Site with $\Psi_T$ Pocket .....	28
14. Rooperol docked on p38 $\alpha$ structures 1LEW and 2OZA.....	30
15. Rooperol docked on p38 $\alpha$ structures 2Y8O and 2OKR .....	31
16. Rooperol docked on p38 $\alpha$ structures 3GT1 and 2ONL .....	32
17. Rooperol docked on p38 $\alpha$ structures 5UOJ and 2LGC .....	33
18. Rooperol docked on p38 $\alpha$ structure 1A9U .....	34
19. Rooperol Analogue Scheme .....	35

20. Rooperol Analogue D1D1 docked on 1LEW .....	37
21. Highest predicted binding energy rooperol analogues docked on 1LEW .....	38
22. Highest predicted binding energy rooperol analogues' interaction with ARG 136.....	39
23. Cytotoxicity tested rooperol analogues resulting pose within DRS pocket.....	41
24. Cytotoxicity tested rooperol analogues pose interaction with ARG 136.....	42

## LIST OF ABBREVIATIONS

<b>Abbreviation</b>	<b>Description</b>
MAPK	Mitogen-activated protein kinase
MAPKK	Mitogen-activated protein kinase kinase
MAPKKK	Mitogen-activated protein kinase kinase kinase
DRS	D - Recognition Site
ATP	Adenosine triphosphate
ADP	Adenosine diphosphate
ATF2	Activating transcription factor 2
KIM	Kinase Interaction Motif
ELISA	Enzyme-linked immunosorbent assay
PBS	Phosphate buffer saline
DTT	Dithiothreitol
ARG	Arginine
ASP	Aspartate
RMSD	Root mean square deviation

## ABSTRACT

Cancer therapeutic drugs have evolved over time in correlation with the understanding of the biological mechanisms which they affect. Many anti-cancer leads have been found in natural sources. The African potato, *Hypoxis hemerocallidea*, is widely used in South African as a medicinal plant for the treatment of cancer and other diseases. Extracts from the corms of this plant contain the major biologically active component hypoxoside. Hypoxoside is hydrolyzed to the anti-cancer agent rooperol ((1,5-bis(3',4'-dihydroxyphenyl) pent-1-en-4-yne) which has been shown to inhibit cancer cell lines. In a Phase I clinical trial, lung cancer patients showed promising anti-cancer activity results, with one patient cancer free after 5 years. Rooperol is metabolized into biologically inactive forms with glucuronic acid and sulfates groups. Analogues of rooperol have been synthesized with the goal of increasing metabolic stability while preserving anti-cancer activity. Rooperol has been seen to inhibit microtubule formation as well as inhibit mitogen-activated protein kinase p38 $\alpha$  which is known to influence control of the cell cycle, inflammation, and cancer.

The goal of this research was to investigate the ability of rooperol and analogues to inhibit p38 $\alpha$ . The study used *in vitro* ELISA and luminescent ADP assay to quantify kinase activity. Then *in silico* docking studies were done to compare analogues and rooperol in binding to p38 $\alpha$ . With this docking information in correlation with cytotoxicity to identify possible anti-cancer or anti-inflammatory compounds.

## I. BACKGROUND

### Natural Product Anticancer Agents

For the greatest efficacy in complex biological systems, a drug candidate needs to overcome the barriers of diffusion, membranes, and metabolism<sup>1</sup>. The advantages of natural products are that evolutionary pressure has created molecules formidable for use in biological systems<sup>2</sup>. Plants are adept in the creation of secondary metabolites, molecules created for variety of uses such as communication, deterrents, and attractants<sup>3</sup>. Many of these volatile molecules overcome the barriers of diffusion and are highly selective in purpose; qualities highly desirable for possible drug candidates<sup>4</sup>. Natural products have been in use since ancient times, as seen with Dioscorides' list of herbs and their uses in 500 BC, and through the longtime dependence of tribal medicine on key plants. Through the initial focus on plants used in tribal medicine, sources have broadened to marine organisms and microorganisms<sup>5</sup>.

Sourcing natural products from plants, marine life, and microorganisms, with various environment stimuli gives rise to large array of structures and targets with which these molecules interact<sup>2</sup>. In addition to the specificity, natural products have been shown to be less toxic to normal cells and have alternative modes of promoting cell death<sup>6</sup>. Over 40% of cancer drugs approved by the FDA are either natural products or derived from natural products and synthesis<sup>5</sup>. In the World Health Organization list of essential medicines for cancer treatment 11 are natural products or natural product derivatives<sup>7</sup>. Some examples of effective anti-cancer natural products include paclitaxel and irinotecan, both of which have been used to treat multiple cancers including breast, ovarian, lung, bladder, and colon cancers<sup>8</sup>.

Some examples of natural products with varying cellular targets include vincristine, paclitaxel, irinotecan and homoharringtonine. Vincristine is derived from the leaves of the Madagascar periwinkle, and interferes the assembly of the mitotic spindle<sup>6</sup>. Paclitaxel is derived from the bark of the Pacific yew, and affects the assembly of beta-tubulin in microtubules<sup>6</sup>. Irinotecan is derived from Chinese ornamental tree and inhibits topoisomerase I<sup>9</sup>. Homoharringtonine is isolated from the Japanese plum-yew and inhibits protein translation by binding to the A- site in ribosomes<sup>6</sup>.

Finding a drug which interacts and specifically targets cancer cells both *in vitro* and *in vivo* may still have issues when translated to clinical use. First there are side effects, both general and specific, and secondly an issue with resistance. Cancer cells with dynamic altering of the genome have an increased variety between cells within a tumor, this variety may affect those cells susceptible to drug interaction, but not affect those with genetic variants that make them less susceptible<sup>10</sup>.

## **Rooperol**

In South Africa, the African potato, *Hypoxis hemerocallidea*, is widely used in traditional medicine and has been used to treat a variety of ailments including cardiac diseases, parasites, cancer, and testicular tumors<sup>11</sup>. The corms of this plant, an underground rootstock, have been tested, and the major biologically active component found in the corms is the bis-glycoside hypoxoside seen in Figure 1<sup>12</sup>. The hydrolyzed product of hypoxoside is rooperol ((1,5-bis(3',4'-dihydroxyphenyl) pent-1-en-4-yne)<sup>12</sup>.

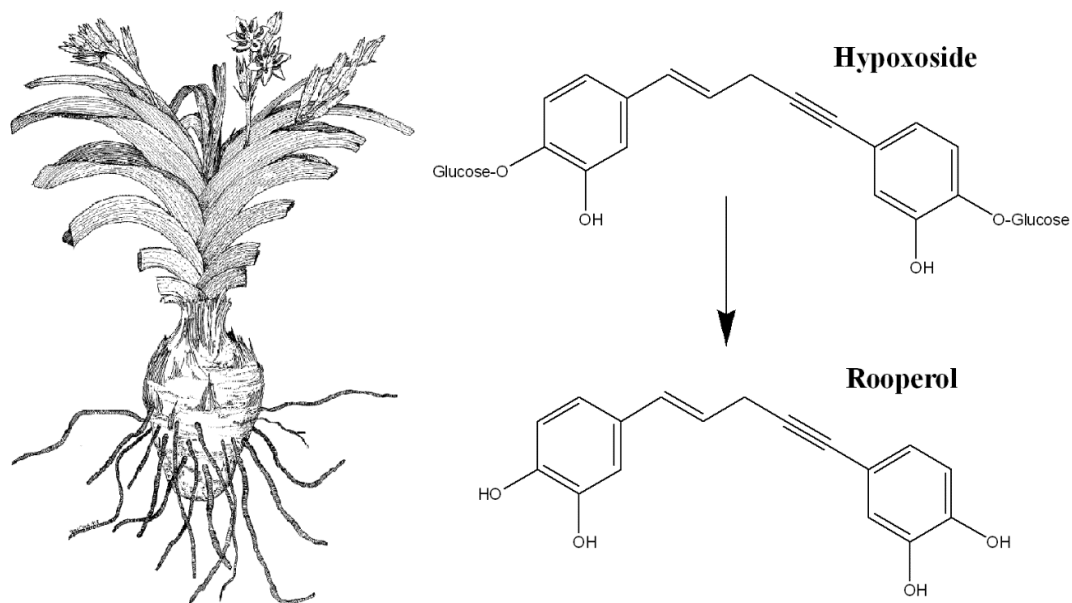


**Figure 1. African Potato and Conversion of Hypoxoside to Rooperol.** Source: Drawing by Dr. Tanza Crouch<sup>13</sup>; the conversion of hypoxoside to rooperol.

Both hypoxoside and rooperol were tested for *in vitro* activity against cancer cell lines and only the latter showed anticancer properties<sup>14</sup>. This trend is also seen in cytotoxic concentration, as it takes only 2-10  $\mu\text{g}$  of rooperol to show toxicity while it takes over 100  $\mu\text{g}/\mu\text{L}$  to see hypoxoside toxicity<sup>15</sup>. This variance is a key factor in the search for possible tumor selective cytotoxic drugs<sup>16</sup>. Rooperol was screened against 60 human cancer cell lines and was found to inhibit the growth of all cell lines, but especially a non-small-cell lung cancer line, which was 14-fold more sensitive to rooperol than the mean cytotoxicity of the other cell lines tested<sup>15</sup>.

*In vitro* testing found that hypoxoside is converted to cytotoxic rooperol via the enzyme  $\beta$ -glucosidase<sup>17</sup>. The research found that metabolites found in urine, consisting of glucuronides and sulphates, were non-toxic to melanoma cells at high concentration<sup>16</sup>. When these metabolites were supplemented with  $\beta$ -glucuronidase the melanoma cells showed inhibition at low concentrations<sup>16, 17</sup>. This correlation of a non-toxic prodrug

conversion to a potent cytostatic drug found local to the cancer gave promising results towards a therapeutic application. In addition, the results left an opportunity for a prodrug analogue with decreased metabolism but the same efficacy to be the focus of research.

In a Phase I clinical trial, advanced lung-cancer patients were orally dosed with corm extracts. This study found patients' blood contained only phase II metabolites of rooperol with the addition of glucuronic acid and sulphate groups onto the catechols<sup>15</sup>. Results of the study found that one patient was cancer free after five years<sup>15</sup>. It is proposed that tumor with high  $\beta$ -glucuronidase activity convert the glucuronide Phase II metabolites to rooperol<sup>16</sup>. The selectivity of rooperol for stem-like cancer cells is a critical factor to its possible use, as it can be used for adjunct therapy for combatting recurrence successfully<sup>18</sup>.

The potential targets of rooperol are found to regulate the cell cycle at G1/S phase and can be related to the combination of sterols as well as hypoxoside found in the extracts from the plants<sup>14</sup>. Rooperol was found to target different protein structures within the cell including microtubule formation and mitogen-activated protein kinase p38 $\alpha$  (Dr. Mooberry UTHSCSA unpublished). In addition, Li *et al.* found rooperol to directly interact at the D recognition site on p38 $\alpha$ <sup>19</sup>.

### **Mitogen-Activated Protein Kinases (MAPK)**

Mitogen-activated protein kinases (MAPK) are a highly conserved family of protein kinases and are involved in a wide assortment of cellular processes such as cellular growth, replication, differentiation, and apoptosis. These pathways are intricate multi-step interwoven highways from initial signal to response<sup>20, 21</sup>. MAPK pathways are

organized into a three-tier system where a signal causes a cascade of phosphorylation from a MAPK kinase kinase (MAPKKK/MAP3K), to a MAPK kinase (MAPKK/MAP2K) to MAPK as seen in Figure 2.

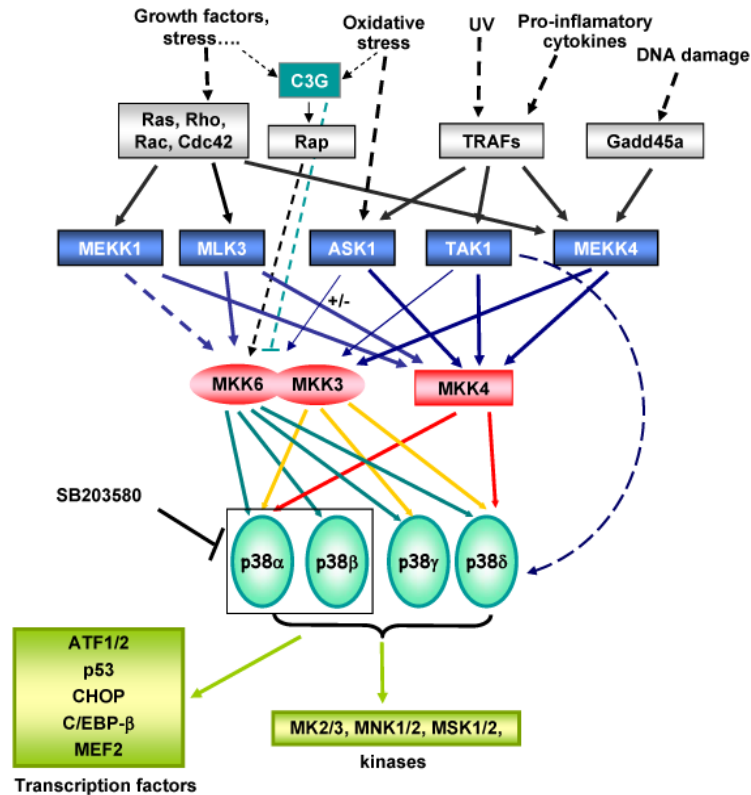


**Figure 2. MAPK pathway.** The upstream and downstream interactions of the MAPK pathway from signal to response. Source: Porras *et al.*, 2011 (20).

MAPKs have a two lobe structure, and at the interface of the two lobes is where the majority of interactions occur including the ATP binding site<sup>22</sup>. The known sites of interaction for p38α include the DFG, ED, CD, Docking groove, A-loop regulatory site, DEF, and Lipid Binding Sites shown in Figure 3<sup>21, 23, 24</sup>. It is through many of these allosteric sites that the specificity is derived as both upstream MAPKK and downstream substrates react with these sites<sup>22</sup>.

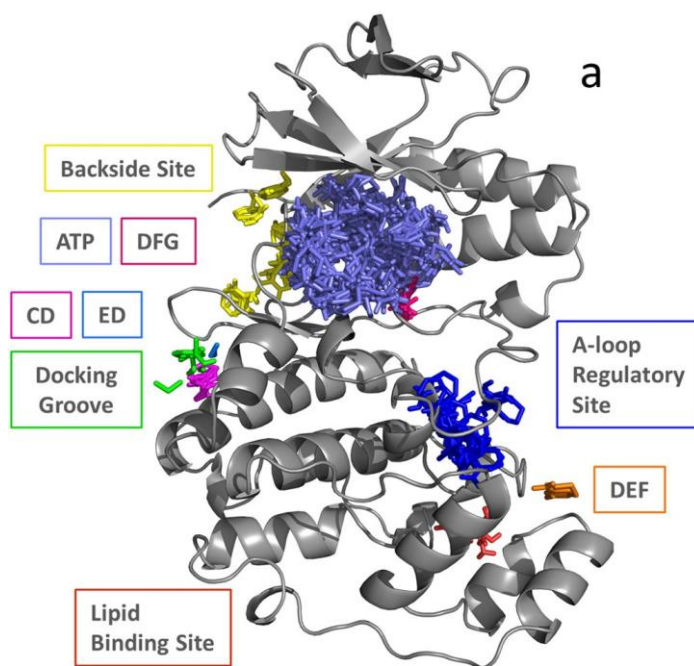


**Figure 3: Docking Sites on P38 $\alpha$ .** Adapted with permission from reference 23: Patricia Gomez-Gutierrez; Jaime Rubio-Martinez; Juan J. Perez; *J. Chem. Inf. Model.* **2017**, 57, 2566-2574. Copyright 2017 American Chemical Society.

The p38 $\alpha$  kinase pathway is of interest due to the pathway's activation in response to stress<sup>25</sup>. The response to stressors has been found to be linked to inflammation, control of the cell cycle, and cancer<sup>26,27</sup>. P38 $\alpha$  is activated by various stress stimuli, through various upstream MAPKKs. These upstream MAPKKs can phosphorylate hydroxyl groups of serine/threonine and tyrosine residues, but MAPKK specifically activates a few MAPKs<sup>28</sup>. The specific action of MAPKK denotes more than the phosphorylated side chain is involved in the specificity of interactions. P38 $\alpha$  recognizes a variety of different proteins based on its structure outside of the conserved ATP binding site<sup>23,29</sup>. These sites function in either regulatory or recognition capacity towards other proteins including transcription factors and downstream kinases<sup>23</sup>.

One of the downstream substrates of p38 $\alpha$  is activating transcription factor 2 (ATF2). This factor forms homodimers that bind a CRE-like recognition sequence, and has been known to be essential in embryonic development as well as the regulation of apoptosis<sup>30-32</sup>. Molecular dynamics run with p38 $\alpha$  identified other druggable sites, which include three novel sites near the lobe interface<sup>33</sup>. Most of the drug candidates under research inhibit MAPKs at the ATP binding site. In contrast, rooperol interacts with p38 $\alpha$  near Cys119 at the docking recognition site (DRS)<sup>19</sup>.

The DRS site has been described in the literature as the KIM, kinase interaction motif, a docking site in the C-terminal lobe of 13-16 conserved residues<sup>34</sup>. The KIM motif has a consensus sequence (R/K)<sub>2-3</sub>-X<sub>2-6</sub>- $\Phi$ <sub>A</sub>-X- $\Phi$ <sub>B</sub> (where  $\Phi$  is any hydrophobic) and is found on many regulatory proteins of MAPKs. The binding groove site is encompassed by six different pockets to compliment the sequence with two electrostatic,  $\Psi$ <sub>U</sub> &  $\Psi$ <sub>L</sub>, and four hydrophobic,  $\Phi$ <sub>A</sub>,  $\Phi$ <sub>B</sub>,  $\Phi$ <sub>L</sub> &  $\Phi$ <sub>U</sub> seen in Figure 4.

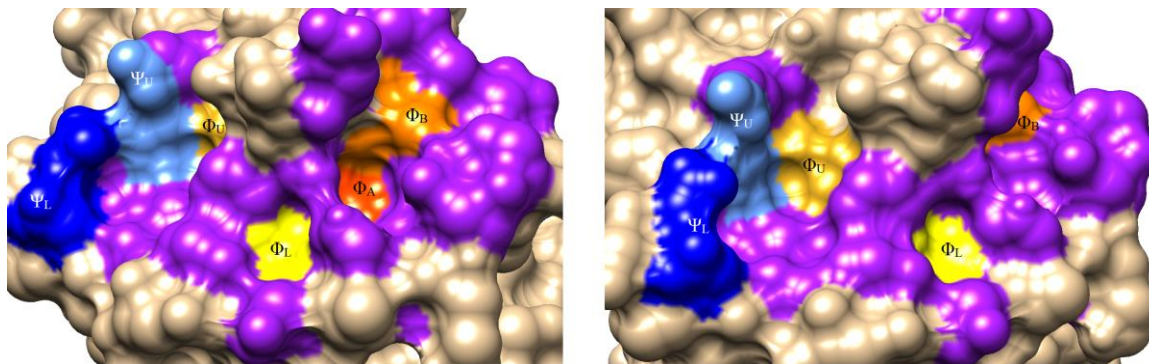


**Figure 4: DRS/KIM Binding Site.** Binding site of p38 $\alpha$  structure (1A9U), showing total binding site in purple, and with labeled pockets  $\Psi$ <sub>U</sub> (light blue),  $\Psi$ <sub>L</sub> (dark blue),  $\Phi$ <sub>A</sub> (red orange),  $\Phi$ <sub>B</sub> (orange),  $\Phi$ <sub>L</sub> (yellow) and  $\Phi$ <sub>U</sub> (gold).

### Rooperol Analogues

With the catechol groups of rooperol undergoing significant Phase II metabolism, a strategy to synthesize rooperol and create analogues with greater metabolic stability

was employed<sup>33</sup>. These molecules retain the backbone structure while replacing different substituents at the catechol moiety seen in Figure 5.

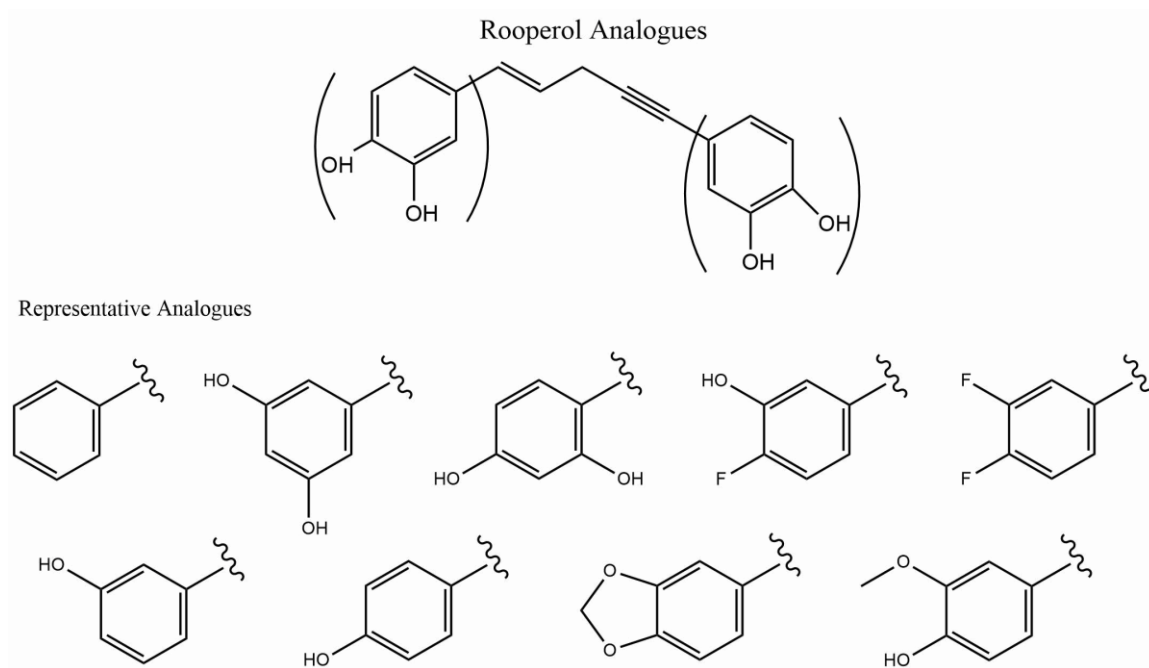


**Figure 5: Rooperol Analogue Overview.** Rooperol is shown with catechol groups in parentheses, where the variation occurs. Below a sampling of catechol replacements that are found in the analogues.

These analogues have been preliminarily tested in cell viability assays and results show varying cytotoxicity levels (Dr. Du & Dr. Kerwin unpublished). In addition, the metabolic stability of rooperol has been tested via *in vitro* metabolism assays. With cytotoxicity, metabolic stability, and the inhibition of p38 $\alpha$  these analogues can be grouped into anti-cancer candidates, and possible anti-inflammatory drugs.

## Research Aims

The goal of this project was to characterize the inhibition of p38 $\alpha$  by rooperol and rooperol analogues. Analogues with increased inhibition were noted and compared to metabolic stability and cytotoxicity data. The results were used to investigate the relationship of p38 $\alpha$  to cytotoxicity in relation to its anticancer activity. Secondly, the results of inhibition along with metabolic stability could identify a product which could be a metabolically stable drug for the treatment of other pathway related phenotypes such as inflammation <sup>35</sup>.

To test these analogues, an *in vitro* inhibition assay was done to quantify rooperol and each analogue's ability to inhibit p38 $\alpha$ . The reactions were done in a system of p38 $\alpha$  and ATF2. ATF2 was chosen for use with p38 $\alpha$  as the full folded protein gives better insight into the allosteric effect of interaction at the docking site on the kinase <sup>36</sup>. An applicable kinase assay was used to test the activity of p38 $\alpha$ . Assays include two types: measurement of ADP, or the measurement of phosphorylated protein. Many of these assay techniques, such as radioactive phosphoprotein measurement, required training for use, as well as specific instrumentation which favored the use of an assay with non-radioactive measurement techniques. This led to the choice of two assays used, an enzyme-linked immunosorbent assay (ELISA) measuring the amount of phosphorylated ATF2 as well as an ADP-Glo<sup>TM</sup> Assay measuring the ADP produced <sup>37</sup>. The phosphorylation of ATF2 correlated to the activity of the kinase and inversely relate to kinase inhibition.

## II. EXPERIMENTAL

### Enzyme-Linked Immunosorbent Assay

#### *Introduction*

To determine the effect rooperol and other analogues would have on kinase activity a screening method was selected. Two products can be quantified from a kinase reaction: phosphorylated protein and ADP. With a high-throughput method, multiple compounds could be tested in one experiment. Additionally, non-radioactive techniques were selected with greater priority. With these two constraints, an ELISA was chosen to quantify phosphorylated protein. From previous work the location and inhibition of rooperol with p38 $\alpha$  is known, but analogues have yet to be determined.

An enzyme-linked immunosorbent assay (ELISA) is used primarily to elucidate detection of proteins, antibodies, hormones, and other molecules. The ELISA works by immobilizing an antigen to the surface of a plate, which is detected by an antibody binding reaction. This antibody is conjugated to an enzyme and binds to the antigen with high specificity. The detection of this binding interaction is measured by a spectrophotometric molecule produced by the conjugate enzyme reaction. For the system: the antigen was ATF2, p38 $\alpha$  was used to phosphorylate ATF2, and the antibody was anti-phospho-ATF2 linked to horseradish peroxidase. The binding of the antibody to the antigen is dependent on the phosphorylation of ATF2, therefore the amount of binding was correlated to the activity of p38 $\alpha$ . With rooperol or an analogue added to solution, correlation between activity influenced by the drug and control activity can be compared.

For this system buffers were made with sodium chloride from VWR, potassium chloride from Sigma Fisher, sodium phosphate dibasic heptahydrate from EM science, potassium phosphate monobasic from Sigma Aldrich, Tween 20 from Acros Organic, HEPES from ThermoFisher, magnesium chloride from OmniPure, DL- dithiothreitol (DTT) (99%) from Sigma Aldrich, sodium orthovanadate from Sigma Aldrich and bovine serum albumin (BSA) from Sigma Life Sciences (98%) and all aqueous solutions were prepared with water from a Thermo Scientific Barnstead MicroPure Water Purification System. The immobilized protein, ATF2 and the kinase which phosphorylates it, p38 $\alpha$ , were provided by the Dalby Lab at UT Austin. Lamba phosphatase was acquired from New England Biolabs. The detection antibody, phospho-ATF2-HRP was acquired from Santa Cruz Biotechnology, and the detection reagent TMB, two bottle TMB and H2O2 reagents, was acquired from BD Bio sciences. The plates used for this study were Immulon 2HB 96-well flat bottom clear microtiter plates. The plates were read using a BioRad iMark Microplate reader set to 450nm absorbance.

### *Procedures*

The ELISA was run according to the methods used by Bauer *et al.*<sup>38</sup> then shifted to Gottert *et al.*<sup>37</sup> with a few modifications. ATF2 was prepared in sterile PBS buffer (137 mM NaCl, 2.7 mM KCl, 10 mM Na<sub>2</sub>HPO<sub>4</sub>, 1.8 mM KH<sub>2</sub>PO<sub>4</sub>, pH 7.4) and incubated in the plate while shaken overnight at 4 °C. The following day, the plate was washed 3 times with wash buffer (PBS), then blocked with blocking buffer (PBS, 0.1% Tween 20, 0.25% BSA) for 12 mins and washed 3 times with wash buffer. The kinase was prepared in HEPES buffer (100 mM HEPES pH 6.8, 10 mM MgCl<sub>2</sub>, 4 mM DTT, 0.1 mM Na<sub>3</sub>VO<sub>4</sub>, 1.4  $\mu$ M ATP), and incubated in the plate for 1 hour. After incubation, the plate was

washed 3 times with wash buffer then antibody solution (blocking buffer with 1:60000 dilution of antibody) put into the plate and incubated for 1 hour. The plate was then washed 3 times with PBST (PBS buffer, 0.1% Tween-20) and then drained. The TMB reagent was then added and reaction allowed to proceed for 5 minutes creating a blue color, then 25 uL of 1M sulfuric acid was added to each well stopping the reaction and turning the color to a bright yellow. The plate was then read for absorbance at 450 nm, and the data plotted in Excel.

### **ADP-Glo™ Assay**

#### *Overview*

Kinase activity measurement has long been dependent on radioactive and methods for detection<sup>39</sup>, using <sup>32</sup>P in radioactive ATP to denote the removal of  $\gamma$ -phosphate on ATP. A non-radioactive route was determined due to the necessary training for safety and equipment needed for radioactive assays. The ADP-Glo™ Assay is a non-radioactive assay developed by Promega to quantify the amount of ADP produced in a kinase reaction. The assay works as it creates a detectible luminescence proportional to ADP which can be correlated to the activity of the kinase. The assay uses a two-step process to remove excess ATP and measure ADP found after the kinase reaction seen in Figure 6. The process proceeds as follows: the kinase reaction is run, producing ADP, ADP-Glo™ reagent is added removing excess ATP, Kinase detection reagent is added and turns remaining ADP to ATP and produces light. In the experimental system, kinase reaction is run with two model kinase and substrate systems, hexokinase and glucose as well as

protein kinase A and basic myelin protein. Following the model systems, the reaction will be run with p38 $\alpha$  and ATF2.

### *Materials*

For this system buffer was made with Tris Ultra-Pure purchased from VWR, magnesium chloride from OmniPure, bovine serum albumin from Sigma Life Sciences (98%), and optionally DL-dithiothreitol (99%) from Sigma Aldrich, and dimethyl sulfoxide (ACS grade, 99.9%) from Sigma Aldrich. Protein kinase A and basic myelin protein were purchased from Sigma Life Science, hexokinase purchased from VWR, and p38 $\alpha$  and ATF2 were provided by the Kevin Dalby Lab at UT Austin. Rooperol was synthesized in the Kerwin Lab, as well as CAPA and CAPE analogues. All aqueous solutions were prepared with water from a Thermo Scientific Barnstead MicroPure Water Purification System. Instruments included a VWR Analogue Vortex Mixer, Molecular Devices M3 Spectra Max plate reader, as well as a BioRad ChemiDoc XRS+. ADP-Glo<sup>TM</sup> kit was acquired from Promega, and included Ultrapure 10 mM ATP, Ultrapure 10 mM ADP, 1 mL of ADP-Glo<sup>TM</sup> solution, and 2 mL of Kinase Detection solution. The composition of the Kinase Detection solution contains a luciferase-luciferin enzyme which converts ATP to light.

### *Procedure*

The procedure for the kinase reactions followed the manufacturer's protocol as well as that of Zegoutzi *et al.*<sup>40</sup> with some modifications. The ADP-Glo<sup>TM</sup> Assay was purchased from Promega, and used with Reaction Buffer A (40 mM Tris pH 7.5, 20 mM MgCl<sub>2</sub>, 0.1 mg/mL BSA). Stocks of ultrapure ATP and ADP were diluted from 10 mM provided stock to 500  $\mu$ M. Second, a Percent ADP Conversion curve was created by

pipetting the 500  $\mu$ M solutions in various ratios to show theoretical production by the kinase seen in Table 1; 0% solution contained ATP, 50% contained 10  $\mu$ L ATP & 10uL ADP, and 100% contained ADP. Substrate solution was created to include 500  $\mu$ M ATP, and appropriate concentration of substrate.

**Table 1. Volumes of ATP and ADP for Percentage Conversion Curve.** The volumes of ADP and ATP combined to create percentage ADP solutions. Both ADP and ATP sources are the same concentration.

<b>ADP %</b>	<b>0</b>	<b>1</b>	<b>2</b>	<b>3</b>	<b>4</b>	<b>5</b>	<b>10</b>	<b>20</b>	<b>40</b>	<b>60</b>	<b>80</b>	<b>100</b>
<b>ADP (uL)</b>	-	2	4	6	8	5	2	4	8	12	16	20
<b>ATP (uL)</b>	20	198	196	194	192	95	18	16	12	8	4	-

Enzymes were diluted to various concentrations and placed into wells with their appropriate substrates and left for one hour to incubate. After incubation ADP-Glo™ reagent was added and incubated 40 min, after which Kinase Detection reagent is added and allowed to incubate 60 min. Luminescence is read at 30 mins and 60 min incubation of Kinase Detection reagent.

## **Molecular Docking**

### *Overview*

Molecular docking is a computational procedure that tries to predict the non-covalent binding of a macromolecule and a small molecule ligand. Starting with two unbound structures, the program calculates force field interactions and results in a predicted binding energy and binding conformation. To further elucidate the interactions of rooperol and analogues with p38 $\alpha$ , as well as help support synthesis efforts, a

docking of all the analogues was performed on p38 $\alpha$  and docking rooperol on various p38 $\alpha$  structures was done. Autodock Vina functions by determining a bound conformation preference and free energy. This is accomplished via an empirical scoring function to evaluate conformation and binding energy between molecules, and applies a stochastic sampling for optimization.

### *Materials*

p38 $\alpha$  files were downloaded from the Protein Databank (rcsb.org) and p38 $\alpha$  structures used included 1LEW<sup>24</sup>, 2Y8O<sup>41</sup>, 2OZA<sup>42</sup>, 2ONL<sup>43</sup>, 2OKR<sup>43</sup>, 2LGC<sup>44</sup>. Software used included Autodock Tools from MGL Tools<sup>45</sup> 1.5.7, Autodock Vina<sup>46</sup> 1.1.2, and UCSF Chimera<sup>47</sup> 1.14 and ChemDraw Prime 17.1 ©Perkin Elmer Informatics.

### *Procedure*

Rooperol and other drugs were drawn using ChemDraw and made into a 3D file via SMILES line structure building in Chimera. The structure was then minimized in Chimera via GAFF force field, Antechamber<sup>48</sup> charge calculation to the nonstandard structures, and AM1-BCC bond charge correlation, and saved as mol2 files. The routine for minimization was run using structure minimization in Chimera selecting: default minimize structure settings with adjusting the conjugate gradient steps to 1000, accepting add hydrogen for docking default settings, assigning charges via AM1-BCC with adding labels showing charges to nonstandard residues, and selecting the overall net charge of the molecule. For better comparison of the various analogues and p38 $\alpha$  files using Chimera all of the p38 $\alpha$  structures were overlaid with 1LEW using the Chimera mm command and saved in the orientation such that the same box could be used for all the proteins. In AutoDock Tools, the PDB file of the protein was prepared by removing water

molecules, adding polar hydrogens, removing non-bonded atoms, and removing any ligands or replicate protein chains. Specifically, 1LEW at the C terminus had residue changed as it included a non-bonded oxygen. After selecting the protein as macromolecule for grid, it was saved as a PDBQT file, then the grid box size and location was determined to cover the area in which docking will take place using the Grid Box function in AutoDock Tools. The ligand molecule is prepared by assigning which bonds are rotatable and non-rotatable in AutoDock Tools and saved as a PDBQT file. A run file was created using a text editor and denoted the ligand and protein files, the box center location (33.33, 44.973, 20.025), dimensions (18.0, 20.0, 28.0), and exhaustiveness 32. Then invoking the program via the command line, the docking was run with AutoDock Vina and the created two resulting files, a PDBQT and OUT. The PDBQT file gives locations and poses of the results of the run, and the OUT file shows the pose, affinity and RMSD values. The resulting interaction was viewed by opening both the protein and the resulting PDBQT files with poses of the ligand. The affinity value in kcal/mol denotes a binding energy, and the RMSD, root mean square deviation, denotes changes in the poses compared to the most favorable energy pose.

### III. RESULTS AND DISCUSSION

#### ELISA

The initial work done for ELISAs involved optimization plates which focused on establishing conditions which would be appropriate for determination of small changes in enzyme activity due to drug inhibition. For assay to be used the following conditions needed to be met: low standard deviations of replicates (<10%), a high signal to noise ratio, and reproducibility. The first experiments focused on determining the substrate range, by varying the amount of ATF2 incubated within the well to the absorbance found at 450 nm. Following the Bauer *et al.*<sup>38</sup> protocol a variation of 100 ug/mL to 0.781 ug/mL was tested in replicate. In efforts to conserve protein, the points with the lower concentration were considered for use, and 12.5 ug/mL met the criteria of smallest standard deviations and appropriate signal-to-background ratio and was selected as seen in Figure 6. The issues present from the initial plates were the lack of variation between the ATF2 incubated with kinase and without kinase, or signal to noise.

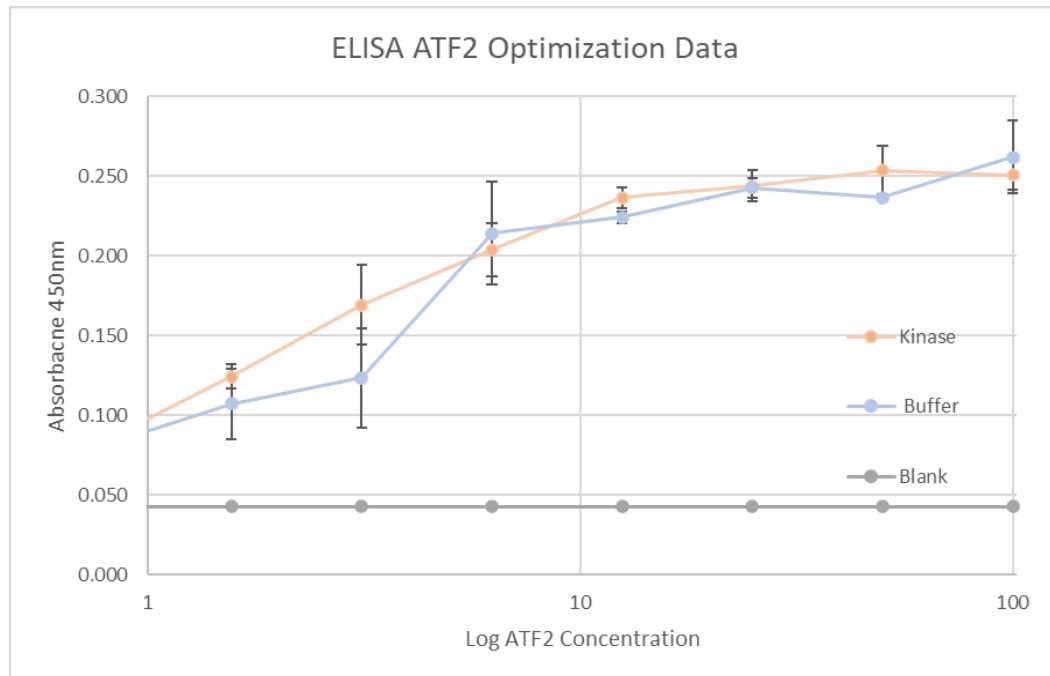


**Figure 6. Signal to Noise Optimization ATF2 Concentration.** ELISA assay run with ATF2 and p38 $\alpha$  showing the signal produced by the assay, and variance between background (gray) and signal (blue and orange).

To address this signal to noise and possibly get greater sensitivity a lower antibody concentration was tested for use. A plate run with 1:300K, 1:60K, and no antibody was run, and results found the 1:300K signal was not above background, and therefore 1:60K should continue to be used. Without a signal with a low antibody ratio, further probing to address signal to noise between ATF2 incubated with and without kinase prompted another possible solution an increase in blocking time.

A plate with increased blocking time showed an improved signal to background but exhibited high standard deviation of replicates. As multiple plates had failed to reach criteria for use, the thought was to eliminate the possible phosphorylation on ATF2 which could be causing the issue. To test variation of phosphorylated and unphosphorylated ATF2 a general phosphatase was acquired, lambda protein phosphatase. Two different plate conditions were tested to probe possible phosphorylation state of ATF2. First the

antigen was bound to the plate, the surface blocked before the phosphatase was used to remove the phosphates possibly present. Secondly, the phosphatase was allowed to react with ATF2 in solution, then the solution was allowed to bind to the plate. Results of the phosphatase incubation before attachment to the plate showed a linear correlation of signal to concentration of ATF2 as shown in Figure 7. This signal present when phosphatase was used confirmed the direct correlated to ATF2, which was not phosphorylated, and at best a signal to noise ratio of 2, and as such another protocol would be tested.

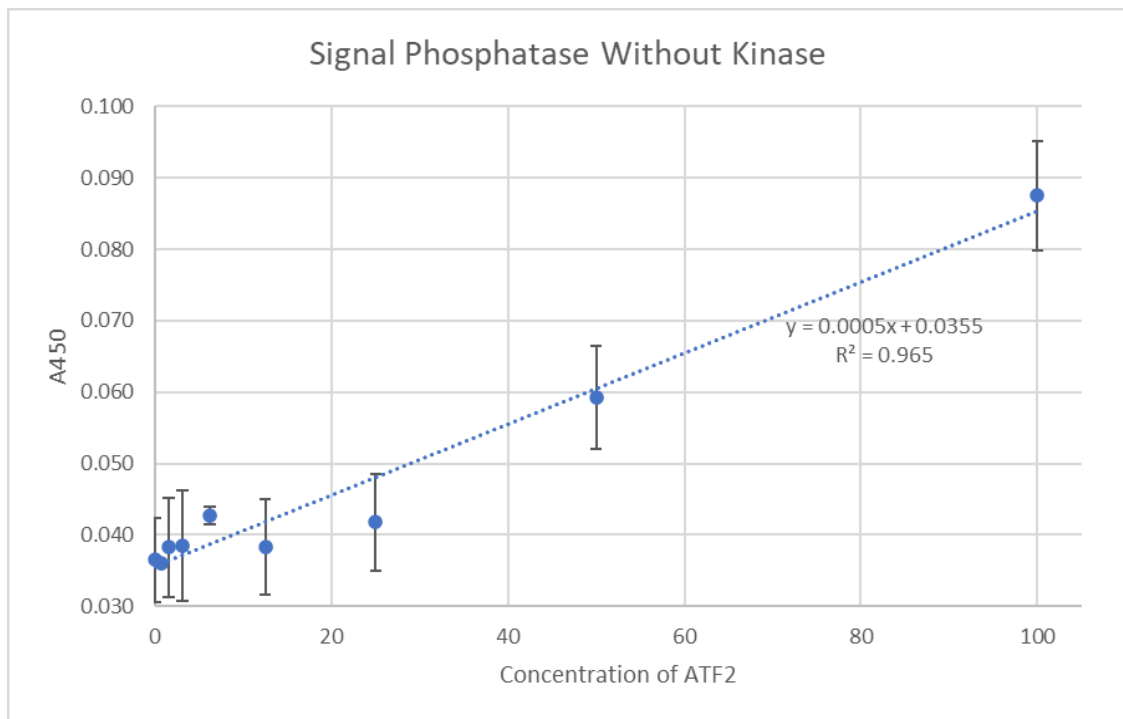


**Figure 7. Signal to Noise Optimization Phosphatase Incubation.** Plate signal produced with by ATF2 alone when incubated with phosphatase and no kinase is present.

After further reading, the methods of Gottert *et al.*<sup>37</sup> was used for its protocols, with variances in washing technique and buffers. The results of the new protocol showed

a positive correlation in signal to increased concentration of ATF2 with a difference in phosphorylated and unphosphorylated protein seen in Figure 8, but despite promising results the lack of low standard deviation of replicates caused the issue of kinase dependence to remain.

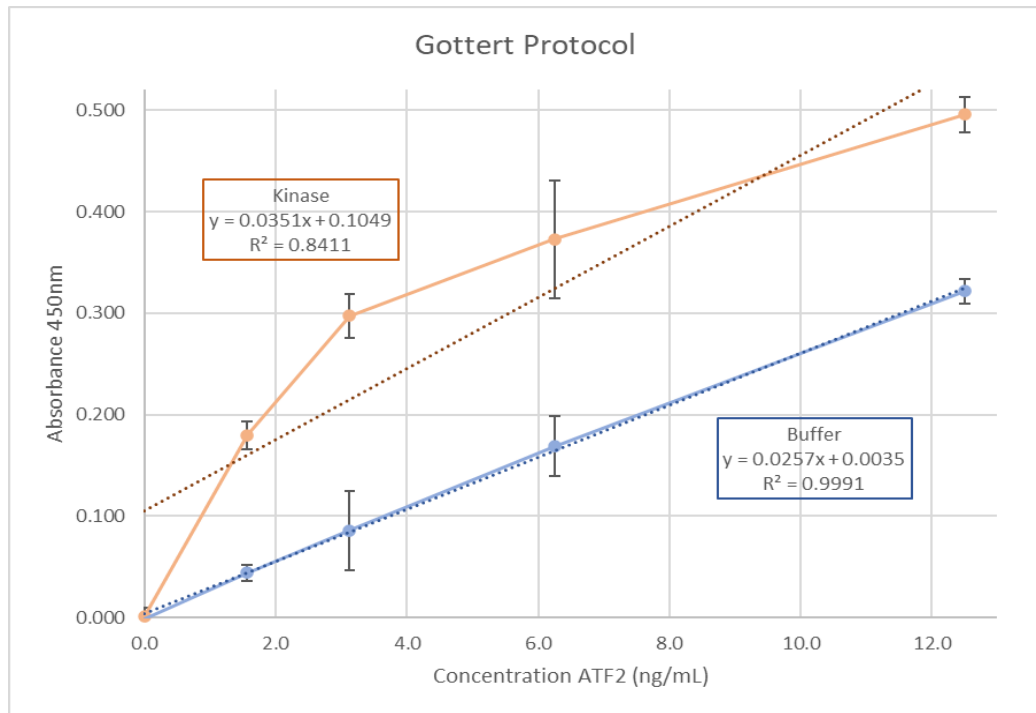


**Figure 8. Signal to Noise Optimization Goettert Protocol.** Initial run with ATF2 and p38a using Goettert protocol to observe possible changes due to washing protocol.

The final experiment run was a kinase dependence assay seen in Figure 9, which with constant ATF2 concentration saw no correlation to kinase concentration. With large standard deviation of replicates and no correlation to kinase concentration. From this point the technique was determined to be not cost or time effective as it had not reach criterion for high throughput assay needed for kinase inhibition testing.

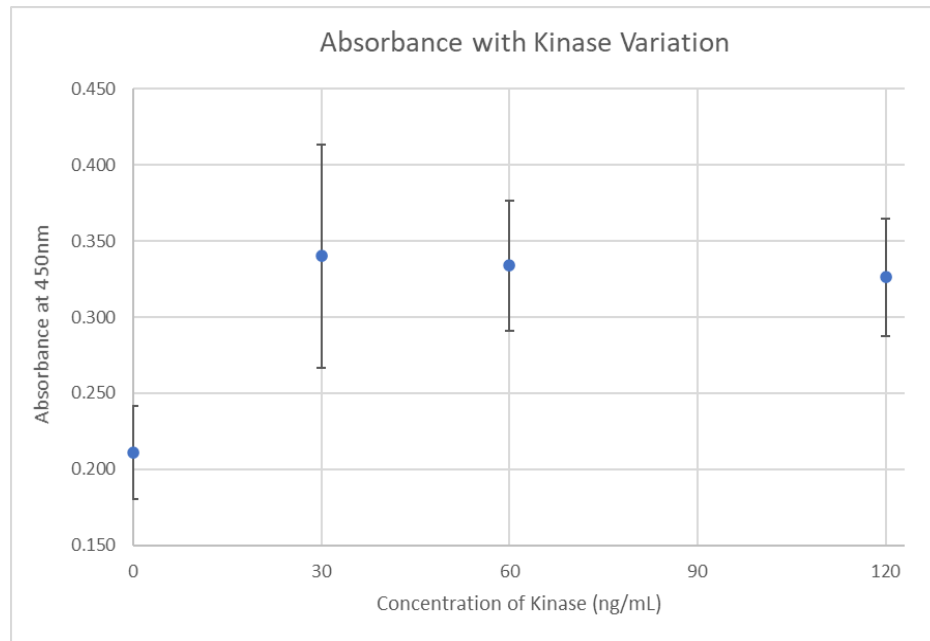


**Figure 9. Kinase Dependence ELISA.** Kinase concentration curve was run using Goettert Protocol with ATF2, and p38 $\alpha$ . Results shows the lack of kinase dependence found in signal.

### ADP-Glo™ Conversion Curve

In switching to a new technique, the goal was to find an assay more universal to measure the activity of various kinases. As such, the focus shifted away from measurement of a specific phosphorylated protein to the production of ADP. A luminescence method was chosen that measures the ADP produced after the kinase reaction with signal produced by luciferase. With this assay high throughput screening criteria were needed for use in further drug inhibition assays such as replicability, low standard deviation of replicates  $<0.1$ , and a large signal to noise ratio. In optimization of this assay, luminescence measured by various ratios of ADP:ATP, and the luminescence observed from kinase reactions carried out over varying concentrations was measured and compared. Taken together, these data were a step-in preparation to quantify the enzyme kinetics for further use with rooperol and measurement of inhibition.

The first step of the technique involved running an ADP conversion curve. This was done to understand the bounds of luminescence signal which could be produced from varying percentages of ADP and to ensure a linear correlation of luminescence signal and percent ADP of various ratios of ADP:ATP at a fixed combined ADP + ATP concentration. Successful generation of this conversion curve would then enable measurement of the approximate activity of the kinase. The bounds of the ADP conversion curve were as follows: if the enzyme did not function no ADP (0%) would be produced and only ATP would reside in solution; if the enzyme reaction ran to completion only ADP (100%) would reside in solution. We initially selected a relatively high (500  $\mu$ M) concentration of ATP for these conversion curves, since if rooperol acts as a DRS-directed inhibitor the inhibition would be independent of ATP concentration. We also limited the volume of the ATP/ADP mixture (5  $\mu$ L) for these curves and the subsequent kinase reactions in order to minimize use of the expensive ADP-Glo™ reagents.

Once a curve was produced with a linear correlation seen in Figure 10, with a signal to noise and acceptable standard deviation of replicates the following step was determination of the enzyme concentration which would be used for the inhibition studies. After testing kinase concentration for activity, the results showed a large difference in the range of luminescence between the ADP Conversion curve and the enzyme concentration curve (data not shown). In an attempt to limit the variability in luminescence data for these curves, the samples for both curves were prepared and assayed simultaneously on the same microtiter plate.

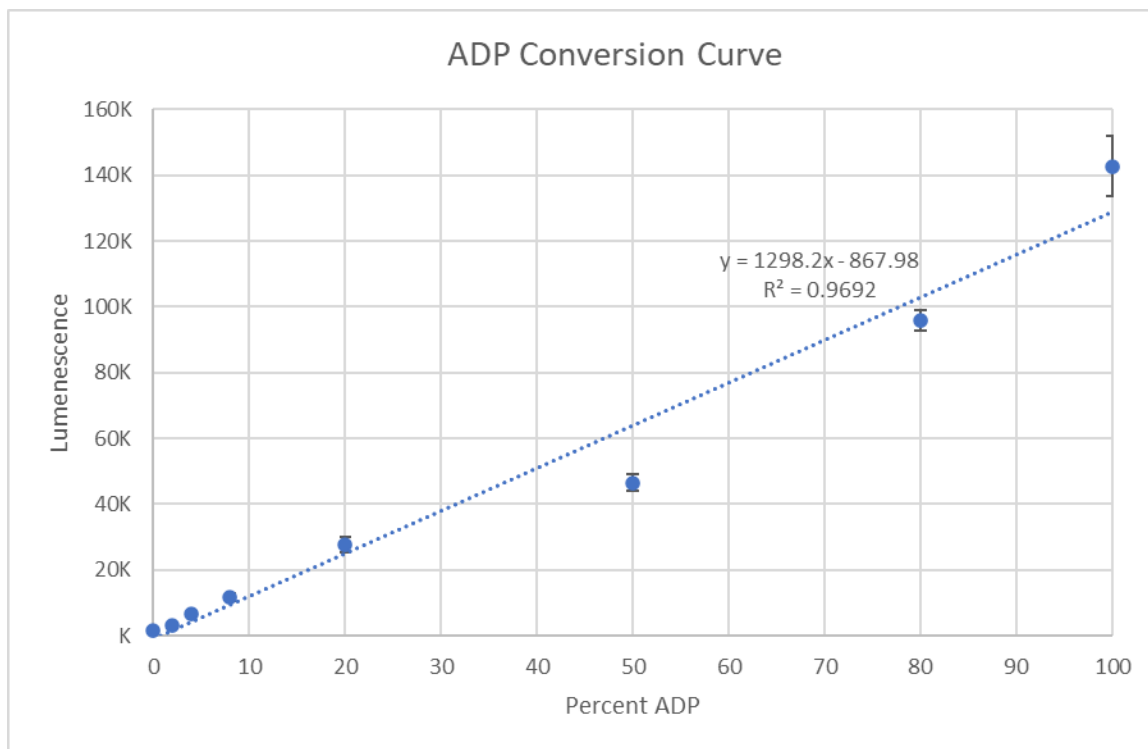


**Figure 10: ADP Conversion Curve with ADP-Glo™ Assay:** The ADP curve run at 500uM of both ATP and ADP made into corresponding solutions, read at 30 mins incubation of detection reagent.

After experiments were done with both curves on the same plate, it was discovered that the ADP conversion curves had issues with large deviations within various ADP percentages. With the large deviations the linear correlation of signal to percentage was unreliable, and therefore the enzyme activity was not quantified. Initially the wells used within the plate were adjusted, skipping both a row and column when pipetting to avoid signal from adjacent wells. With multiple replicates retaining the same issue, it was hypothesized that the ADP-Glo™ reagent was not adequately removing the ATP, and therefore higher signals were seen. After testing two different aliquots of the ADP-Glo™ reagents it was observed that the signal to noise ratio decreased over time and action was then taken to acquire new reagent and to aliquot it for future use.

## **ADP-Glo™ Hexokinase**

After establishing bounds with an ADP percentage curve next was to determine appropriate enzyme concentration. In efforts to cover a variety of kinases, an initial model hexokinase was used for its high activity and inexpensive substrate. To begin hexokinase solutions were made over a range of concentrations from 200  $\mu\text{Units}/\mu\text{L}$  to 0.25  $\mu\text{U}/\mu\text{L}$ . After two experiments converting this range, a 10-fold range was determined for use, from 0.1  $\mu\text{U}/\mu\text{L}$  to 100  $\mu\text{U}/\mu\text{L}$ , and DDT was added to prepare for p38 $\alpha$  buffer conditions. As the various experiments were run, an issue of replicability and precision appeared within both curves but most prominently with the ADP Conversion curve. In efforts to address the replicability, an experiment was repeated seven times.

Data from the replicate experiments showed a consensus of enzyme activity, but the ADP conversion curves between replicates varied significantly as shown in Figure 11 A & B. In the last replicate of the experiment, the plate was pipetted skipping rows and columns between each well with solution, this addressed a portion of the variance but did not reach the precision and accuracy levels desired for the experiment. After various issues with replicability, precision, and reagents but with progress being made, it was determined that this portion of the project would be handed off to another lab member for further optimization and then subsequent use for testing.

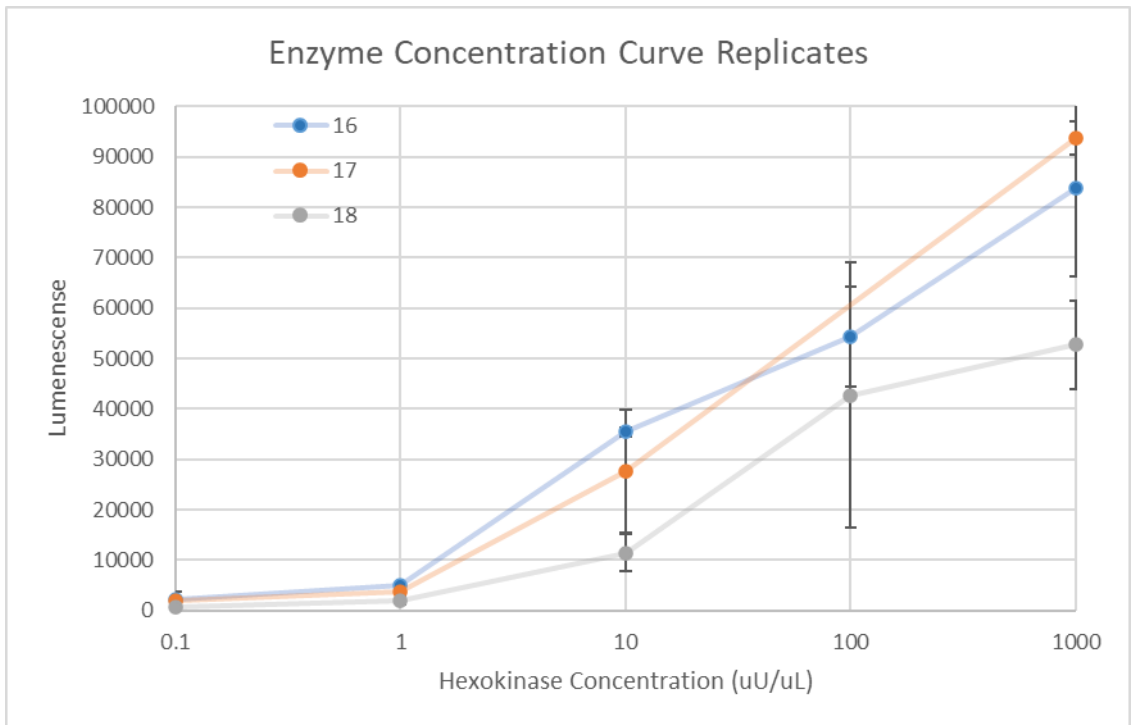
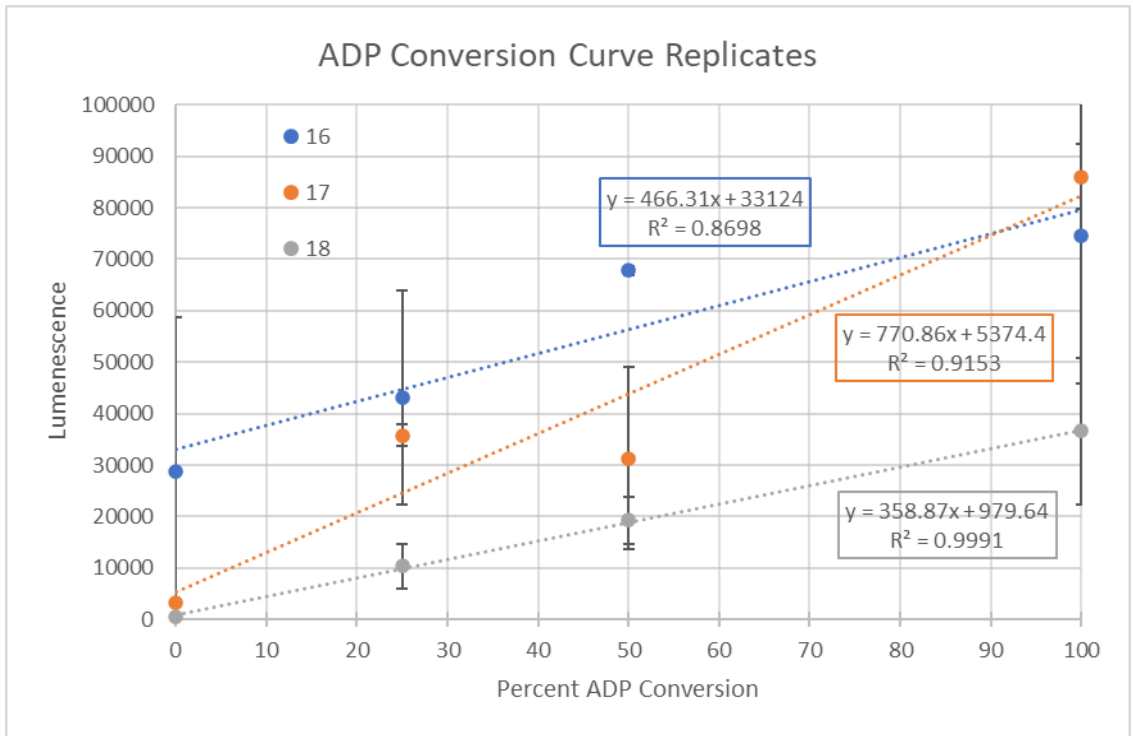


**Figure 11: Hexokinase Enzyme Curve and ADP Conversion Curve**

The graphs show three replicate plates labeled by number, with both the corresponding A) ADP Percentage Curve and B) HK Enzyme Concentration Curve

## Molecular Docking Inhibition Studies

### *Rooperol*

The initial focus of molecular docking was to gain a better understanding of location, pose, and binding energy of rooperol binding to p38 $\alpha$ . With the previous work of Li *et al.*<sup>19</sup> that demonstrated rooperol inhibition of p38 $\alpha$  at the DRS, and the selective DRS inhibition of other structurally similar natural products, this led us to focus on DRS site for initial dockings. The secondary focus was to compare those quantities between rooperol and various analogues. With this information efforts could be focused for synthesis of selected analogues for *in vitro* work, and a better grasp of binding interactions and properties which could improve future drug candidates.

First docking session was done with rooperol and the p38 $\alpha$  structure 1LEW, and viewing the results it was discovered the location of binding was the ATP binding site, and rooperol bound with a relative high binding energy, labeled in Vina output as affinity, of -6.1 kcal/mol. This was an informative result as the energy for ATP site could be compared to any allosteric site noting any with an equal or greater affinity for rooperol. Docking was done using AutoDock Vina, which involves a protein and ligand files as well as a box in which docking will be performed. This box is denoted by dimensions and an origin and denotes the space in which the ligand will be placed to simulate docking. As the docking is stochastic, it can be carried out with varying levels of exhaustiveness to increase the number of positions and interactions being sampled and ensure identification of the most favorable pose.

We next shifted to our focus to docking rooperol to the portion of the DRS near Cys119 following the Li *et al.*<sup>19</sup> probe results. Docking was carried out with varying the

exhaustiveness values, and since there was little differences in the poses, an exhaustiveness value of 32 was selected for all docking studies. With multiple dockings of rooperol at this portion of the DRS on 1LEW the highest binding energy hovered around -4.0 kcal per mole, and the pose remained centered around the  $\Phi_A$  &  $\Phi_B$  pockets. These results would suggest that rooperol is an ATP competitive inhibitor; however, we realized that we had not explored rooperol's interaction with the entire DRS. Subsequent docking was performed with an increased box size adjusted to encompass the entire DRS. After docking rooperol to this box which encompassed the entire DRS, the results showed predicted binding energy that was -2.0 kcal/mol more favorable than that predicted for rooperol binding to the ATP binding site. In these results, rooperol is bound further removed from Cys 119 within the DRS, moving into pockets  $\Phi_U$ ,  $\Psi_U$ , &  $\Psi_L$  as shown in Figure 12.

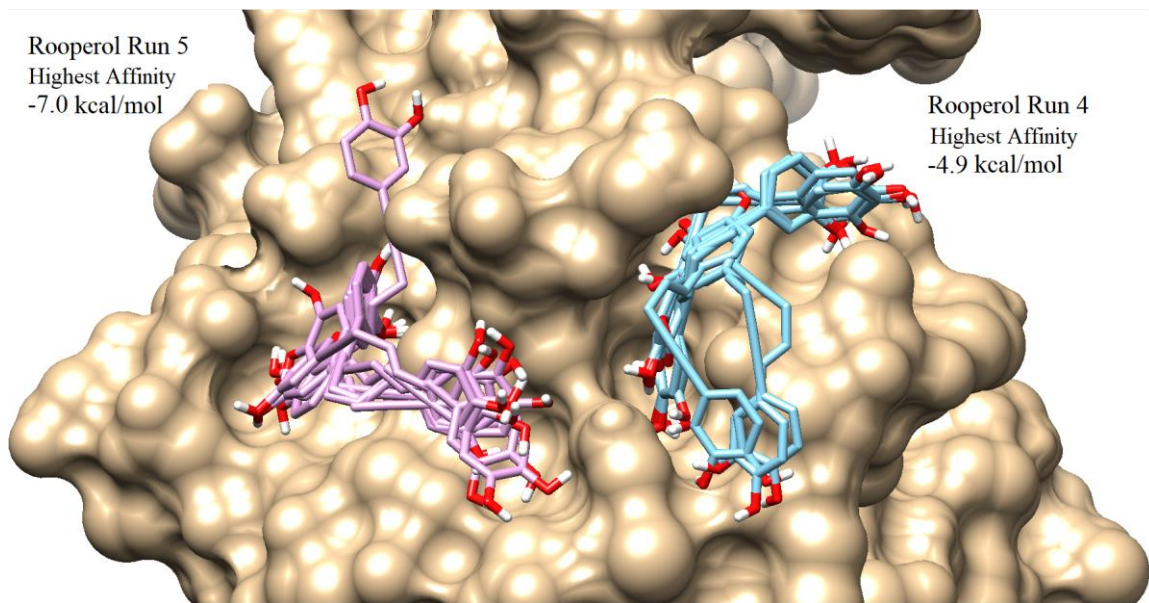


**Figure 12. Initial Rooperol Docking Results.** Two docking results varying box coverage from around Cys 119 (rooperol poses in cyan) to a larger box encompassing the entire DRS (rooperol poses in pink).

Additionally, within run 5 we see a secondary positioning of one rooperol structure into an electrophilic pocket created by Glu163, backbone of Leu164, and Lys165. This pocket, which we will referred to as  $\Psi_T$ , is shown in pink in Figure 13 and is also occupied in further docking results. A sequence alignment was performed to observe the conservation of these residues of the entire site and new pocket and can be found in the appendix.

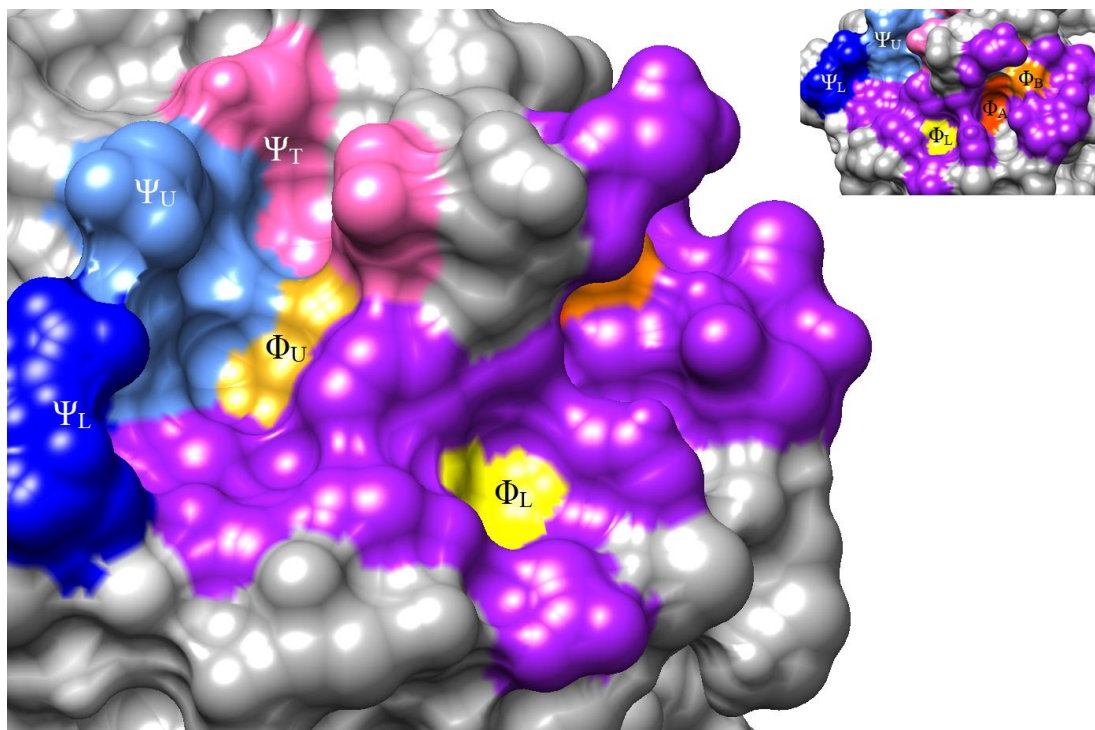


**Figure 13. DRS Site with  $\Psi_T$  Pocket.** The surface of the DRS of p38 $\alpha$  (1LEW) with novel pocket  $\Psi_T$  (pink) and previously identified pockets,  $\Psi_U$  (light blue),  $\Psi_L$  (dark blue),  $\Phi_A$  (red orange),  $\Phi_B$  (orange),  $\Phi_L$  (yellow) and  $\Phi_U$  (gold).

To explore the possible binding modes that may influence where in the DRS rooperol could bind, various p38 $\alpha$  structures with peptide/protein ligands bound to the DRS were acquired in which the ligand binding modes varied. As described in Peti and Page, the proteins binding to p38 $\alpha$  have directionality of binding within the DRS in either a N $\rightarrow$ C or C $\rightarrow$ N direction within the pocket. We selected two pairs of structures in

which the ligands were bound in opposite directions: 1LEW (N→C) and 2OZA (C→N) both mouse structures, 2Y8O (N→C) and 2OKR (C→N) both human structures. In addition, a third pair of mixed binders 3GT1 and 2ONL, one mouse and one human, from were tested. The mouse and human sequences of the protein vary by 3 residues, all of which are outside the DRS site and shown in the appendix. Initial set up work for the various structures found it difficult to encompass the DRS within the box, therefore all the various p38 $\alpha$  structures were oriented to the same coordinates as 1LEW, and a standard box was created with a set location and size to cover the DRS on all the proteins.

In comparison of the docking results employing 1LEW and 2OZA structures, the rooperol poses with the highest binding energy were -7.1 kcal/mol, and -6.5 kcal/mol respectively. More prominent in the comparison is the lack of  $\Psi_T$  pocket involvement in any poses for rooperol binding with 2OZA. This variance was thought to be correlated to original DRS-interacting protein ligand binding mode: in 1LEW the protein binds in a N→C direction, or left to right within the image shown in Figure 14, having the  $\Psi_T$  site being a more accessible surface as the ligand samples the left portion of the pocket. In contrast, the C→N binding mode of 2OZA, has a greater pocket accessibility for binding on the right of the image in Figure 14, and is inaccessible to interact with the  $\Psi_T$  pocket. This variation in rooperol binding modes may be an important component for selective inhibition of N→C binding ligands versus C→N binding ligands due to the dependence of unstructured nature of the N-terminal end of peptides on the conformational changes in their binding site on p38 $\alpha$  as discussed in Garai *et al.*<sup>41</sup>.

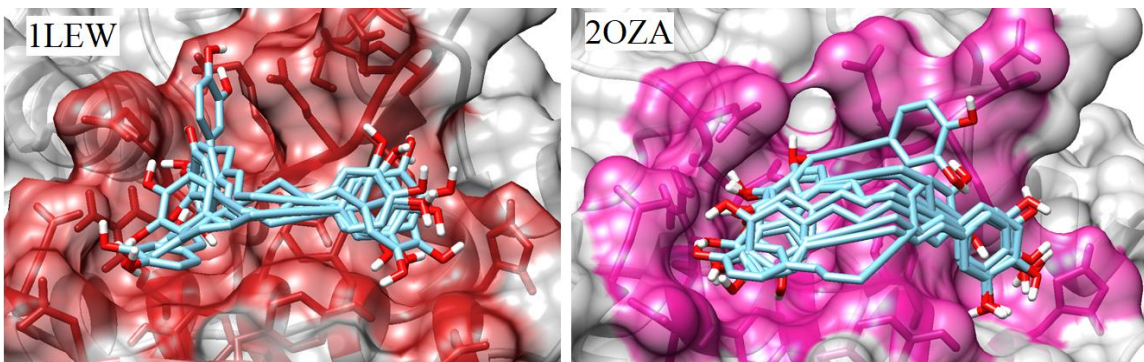


**Figure 14. Rooperol docked on p38 $\alpha$  structures 1LEW and 2OZA** nine resulting poses of rooperol on the respective structures of p38 $\alpha$  are shown in cyan in each frame, with the DRS surface colored red for 1LEW and magenta for 2OZA.

In comparing the rooperol docking results using the 2Y8O and 2OKR p38 $\alpha$  structures as seen in Figure 15, the highest binding energy rooperol poses were -7.0 kcal/mol and -6.5 kcal/mol respectively, and the same pose binding pocket variance occurs with this second set of protein structures. The structure 2Y8O with N $\rightarrow$ C ligand binding direction results in rooperol interactions with the upper  $\Psi_T$  pocket, while the 2OKR structure in which the ligand binds in the C $\rightarrow$ N direction does not have any predicted rooperol interactions with the  $\Psi_T$  as a pocket. However, in this case multiple docking poses have rooperol interacting with two electronegative residues at top of the DRS. Thus, in this structure from a C $\rightarrow$ N bound ligand, the right-hand side of the DRS in Figure 15 is more open to accommodate the unstructured *N*-terminal peptide region, allowing rooperol to interact with the p38 $\alpha$  ASP 161, which stabilizes intra-peptide hydrogen bond staples in C $\rightarrow$ N peptides as described in Garai *et al.*<sup>41</sup>.

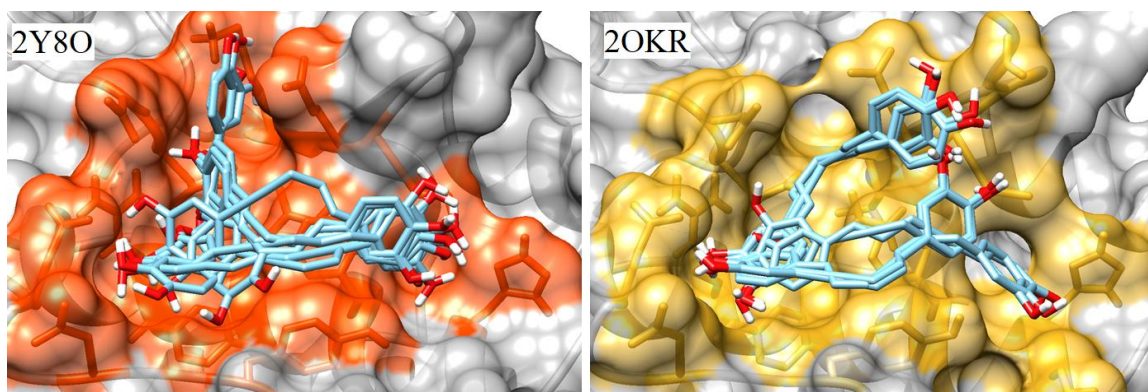


**Figure 15. Rooperol docked on p38 $\alpha$  structures 2Y8O and 2OKR.** Results from Autodock Vina showing nine rooperol poses of predicted binding on the respective structures, labeled in top left, of p38 $\alpha$ . The docking site residues in proximity of rooperol poses are colored to denote different surface interactions

Finally, in comparing the docking results with the p38 $\alpha$  structures 3TG1 and 2ONL, which are complexes with mixed direction binders, respective highest binding energy rooperol poses were -6.5 kcal/mol and -6.6 kcal/mol. In both these particular structures, the DRS has spread out and the pockets have more distance between them, this may be a results of the mixed binding nature of the structures as it improves initial sampling of the ligand but not a predicted higher binding energy for rooperol. In the docking with 3GT1, two predicted rooperol poses interact with ASP 161, which indicates that interactions with rooperol for this structure are more similar to that of p38 $\alpha$  with N $\rightarrow$ C binding ligands, although  $\Psi_T$  is not directly engaged in this case. In contrast, results from docking on 2ONL indicates a rooperol poses similar to those observed in docking to p38 $\alpha$  structures of C $\rightarrow$ N binding ligands as seen in Figure 16. Again, the sampling of rooperol structures to this ASP 161 may more aptly be able to block inter-protein hydrogen bonds to block that interaction.

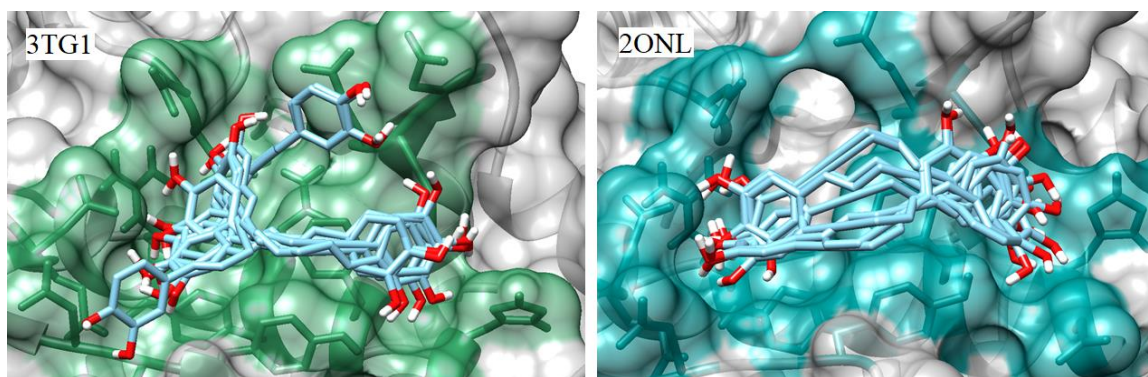


**Figure 16. Rooperol docked on p38 $\alpha$  structures 3TG1 and 2ONL.** Results from Autodock Vina showing nine rooperol poses of predicted binding on the respective structures, labeled in top left, of p38 $\alpha$ . The docking site residues in proximity of rooperol poses are colored to denote different surface interactions

From the mixed binder results, it is hypothesized that 3 interactions influence the binding of rooperol to p38 $\alpha$ , and therefore affect inhibition. These interactions include: the accessibility of  $\Phi_L$  and  $\Phi_U$  pockets and the surface between them, the area between the two  $\Psi$  pockets at ARG 136, and the interaction with ASP 161. The availability of these pockets and areas is optimized in structures from with N $\rightarrow$ C binding ligands, leads us to believe as each interaction in combination makes rooperol effective, and focus on specific interactions could improve specificity of inhibition.

In order to further explore the poses of rooperol, docking was also done on a few other structures 5UOJ, 2LGC and 1A9U. 5UOJ is a high resolution structure which has superseded the initial crystal of p38 $\alpha$ , and 2LGC is an NMR derived structure, with 1A9U being crystalized with a known ATP inhibitor SB203580 bound. With these structures the DRS binding site is unoccupied, and docking studies on these were carried out to see if the rooperol would recognize the shape of the DRS as it exists before protein ligand binding.

With the initial two structures, 5UOJ and 2LGC, the highest binding energy rooperol poses were -7.3 kcal/mol and -6.7kcal/mol. In both structures the highest

binding energy pose was the singular pose which interacts with the  $\Psi_T$  pocket, and in the case of 5UOJ, an additional pocket above as seen in Figure 17. It is hypothesized that another location could be tested after the results seen with 5UOJ, as there may be an upper location for rooperol to bind, which interacts with  $\Psi_T$  and  $\Phi_B$  above the DRS.

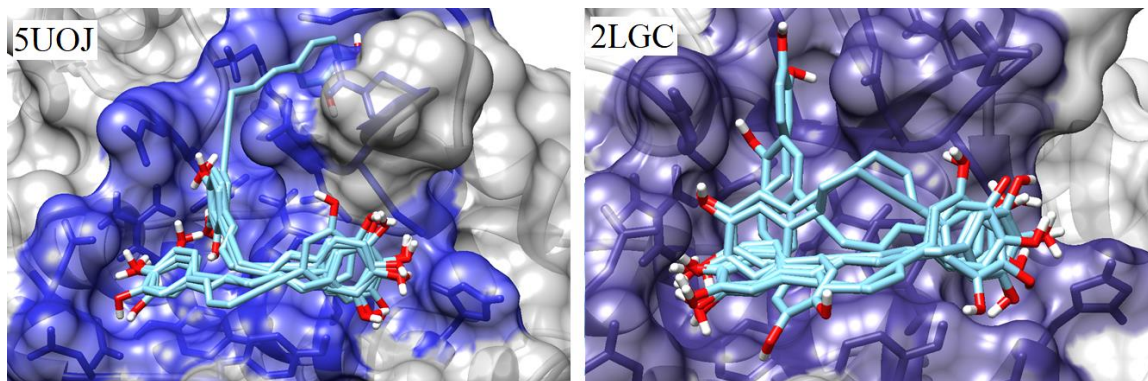


**Figure 17. Rooperol docked on p38 $\alpha$  structures 5UOJ and 2LGC** Results from Autodock Vina showing nine rooperol poses of predicted binding on the respective structures, labeled in top left, of p38 $\alpha$ . The docking site residues in proximity of rooperol poses are colored to denote different surface interactions

Lastly, the structure 1A9U was tested, in which p38 $\alpha$  was bound to ATP inhibitor SB203580 seen in Figure 18. With a highest predicted binding energy of -7.2 kcal/mol, the interaction of rooperol with this structure is comparable to many of the p38 $\alpha$  structures which rooperol binds into  $\Psi_T$  pocket. Due to the similar poses, lack of interaction with  $\Psi_T$ , but favorable binding energy it is believed that the binding of an ATP competitive inhibitor must have a cooperative effect influencing the DRS site and make it higher binding energy site for rooperol. This hypothesis could support a model in which rooperol binds to the ATP binding site, which increases the binding energy for the DRS. Once a second rooperol binds to the DRS, the rooperol in ATP site can be released, while allosteric inhibition of p38 $\alpha$  is retained. This is supported by results of Li *et al.*<sup>19</sup> with an observed the increase of adduction of their probe to the DRS site in the

presence of SB203580, and a second ATP competitive inhibitor, denoting a possible cross-talk of the DRS and ATP binding sites.

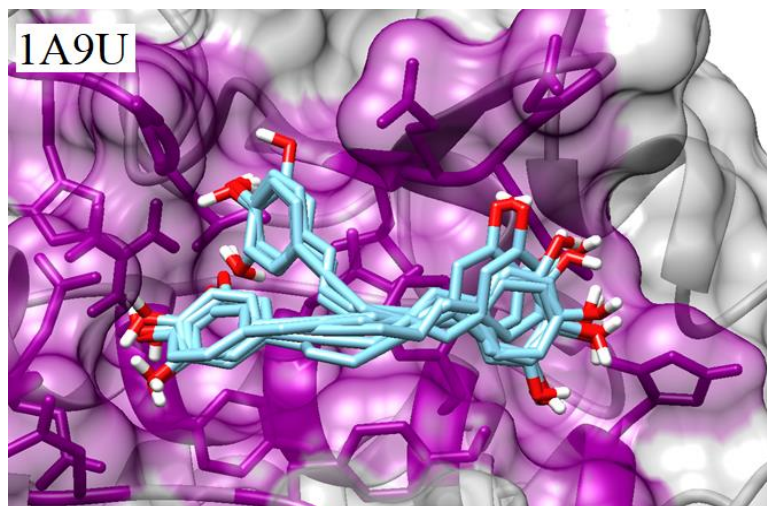


**Figure 18. Rooperol docked on p38 $\alpha$  structure 1A9U** nine resulting poses of rooperol on the structure of p38 $\alpha$  in which the ATP competitive inhibitor SB203580 is bound in the crystal structure 1A9U.

### *Analogues*

The promising results of rooperol in the Phase I clinical trial made rooperol a target for anti-cancer drug research and prompted the focus to understand mechanism and improving results via synthesis of analogues. As such the Kerwin Lab has focused efforts on synthesis of analogues and has created a number of rooperol analogues for further screening. 1LEW was the chosen p38 $\alpha$  protein structure due to its reliability in orientation of the box to cover the entire DRS, as well as its use in initial rooperol docking with ATP-binding site. The box center was placed at (33.33, 44.973, 20.025), with dimensions (18.0, 20.0, 28.0), and was used as it covered all the DRS residue surfaces described by Peti & Page<sup>49</sup>. All the analogues found in the Kerwin Lab inventory were viewed for possible use and drawn using ChemDraw Prime. In the process of conversion to a 3D file in Chimera, only a subset of these were successfully

minimized and chosen for docking. When minimization was performed with analogues with TBSO groups, the Silicon atoms did not retain the correct molecular geometry and attempts to fix the issue were unsuccessful. The naming scheme for analogues denotes the alkene-proximal catechol, R, and then alkyne-proximal catechol, R' as seen in Figure 19. As an example, rooperol is named A0A0, as the catechol moiety (3,4-dihydroxyphenyl) is denoted as A0. The subsequent catechol analogue groups are shown in Figure 19 with their identifier label in the center of the aromatic ring.

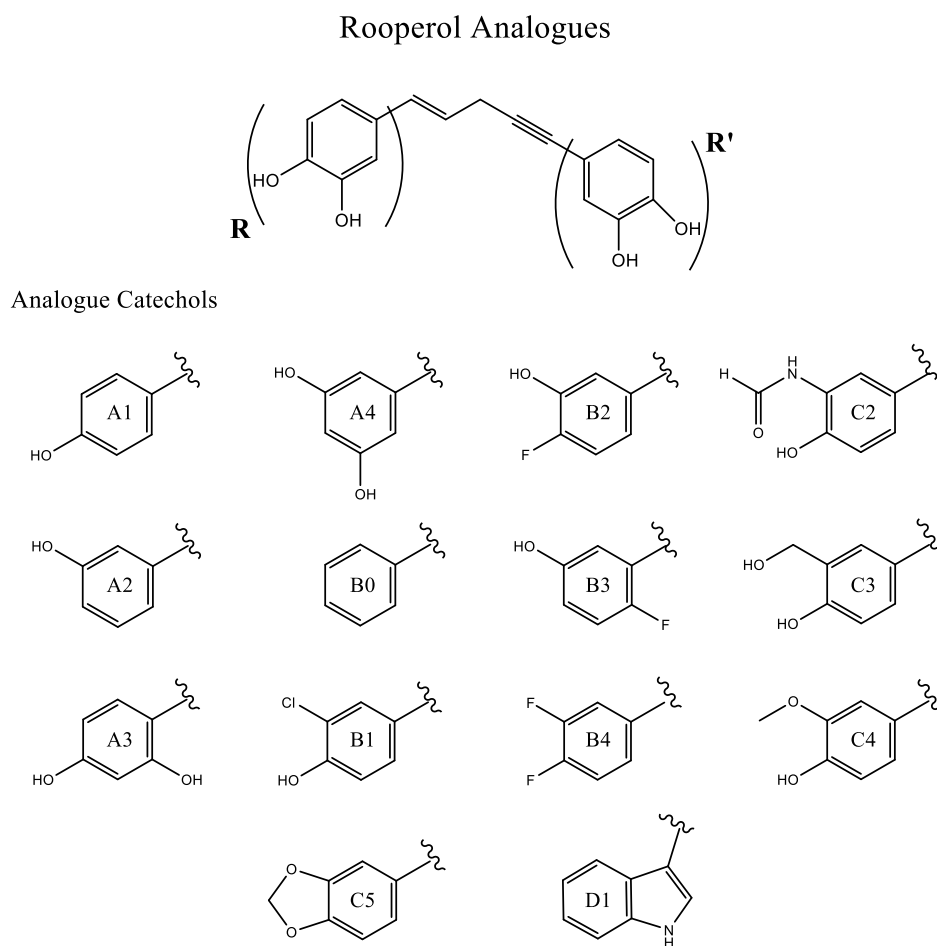


**Figure 19: Rooperol Analogue Scheme.** Rooperol is shown labeling the alkene catechol, R, and the alkyne catechol, R', with initial substituents, A0, on each side. Below the various analogue catechol replacements labeled in the center of the aromatic ring by their identifier.

Rooperol and all analogues were docked onto 1LEW with the box location and size as denoted above. After all the docking was run the highest binding energy pose of each analogue was selected and combined for visual representation and compiled affinities was can be found in Table 2.

**Table 2. Predicted binding affinities of rooperol and analogues docked onto 1LEW**

Analogue	Affinity (kcal/mol)	Analogue	Affinity (kcal/mol)	Analogue	Affinity (kcal/mol)
D1D1	-7.7	A0A0	-7.1	A1A0	-6.9
A0C5	-7.6	A0A3	-7.1	B0A0	-6.9
C5C5	-7.5	A0B2	-7.1	B0B3	-6.9
D1A0	-7.5	A0C4	-7.1	B2B2	-6.9
B0D1	-7.4	B0A2	-7.1	A4B0	-6.8
C5A0	-7.4	B0C4	-7.1	B0B4	-6.8
A0D1	-7.3	B1B1	-7.1	B0C3	-6.8
A2A0	-7.3	C3C3	-7.1	B0C5	-6.8
A3A3	-7.3	C4A0	-7.1	B1B0	-6.8
B0C2	-7.3	D1B0	-7.1	C2B0	-6.8
B3A0	-7.3	A0A2	-7.0	C4C4	-6.8
B3B3	-7.3	A0B0	-7.0	B0B1	-6.7
C2C2	-7.3	A0B1	-7.0	B0B2	-6.7
A0A4	-7.2	A0B4	-7.0	B2B0	-6.7
A0B3	-7.2	A2A2	-7.0	B3B0	-6.7
A0C2	-7.2	A3A0	-7.0	B4B0	-6.7
A0C3	-7.2	A3B0	-7.0	C4B0	-6.7
A4A0	-7.2	B0A3	-7.0	A1A1	-6.6
A4A4	-7.2	B4B4	-7.0	A2B0	-6.6
B1A0	-7.2	C3A0	-7.0	B0A1	-6.6
B2A0	-7.2	C3B0	-7.0	B0B0	-6.5
B4A0	-7.2	C5B0	-7.0	B0A4	-6.5
C2A0	-7.2	A0A1	-6.9	A1B0	-6.4

With the previous understanding of binding direction, the top scoring analogue D1D1, was viewed with a focus on the pocket interactions found at the location of the DRS closest to where the N-terminal end of the protein ligand binds nearest the two electrophilic pockets. Within the docked structure, the orientation of the D1D1 analogue alkene 1H-3-indolyl group, shows the hydrogen in the indole to be positioned at the

bottom of the  $\Psi_L$  pocket as seen in Figure 20. In addition, there is an interaction between this indole NH and the guanidine side chain of ARG 136: the N-H bond is nearly perpendicular to the guanidine plane, with the indole hydrogen located 2.810Å above the guanidine nitrogen. In addition, the aromatic ring of the 1H-3-indoyl group is positioned over the  $\Phi_U$  pocket. On the other end of the molecule the alkyne 1H-3-indoyl group also is positioned 2.666Å from the backbone carbonyl of ASP 161 and the aromatic ring of the indole directly positioned in the  $\Phi_L$  pocket.

The ability of this analogue to interact with both  $\Phi_U$  and  $\Phi_L$  pockets and orient both 1H-3-indoyl groups to additionally be involved in electrostatic interactions are likely reasons why D1D1 exhibited the highest predicted binding energy of the analogues tested.

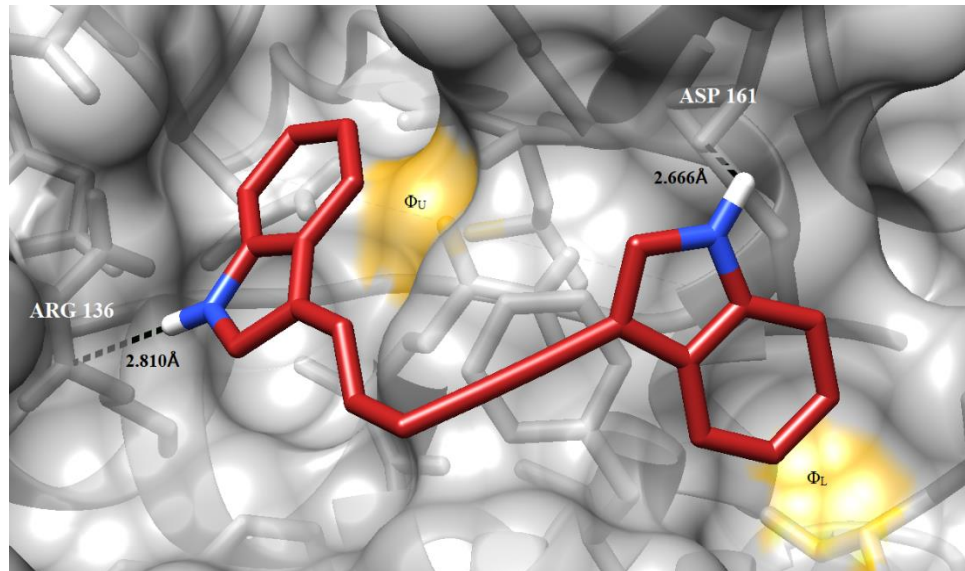


**Figure 20. Rooperol Analogue D1D1 docked on 1LEW.** Analogue D1D1 docking at the DRS site with interactions with ARG136 and ASP 161, and the  $\Phi_U$ , and  $\Phi_L$  pockets shown.

Upon this observation and the knowledge of structure 1LEW being bound to an N→C ligand, it was hypothesized that the docking of all the analogues on 1LEW may favor access and interactions at pockets  $\Psi_L$ ,  $\Psi_U$ , and  $\Phi_U$ , corresponding to the N-terminal side of N->C bound ligands. The higher binding energy analogues would observe a

similar interaction as seen with the D1D1 results. Figure 21 shows the top 6 highest predicted binding energy analogues which all have interaction at  $\Phi_L$ , and  $\Psi_L$  pockets.

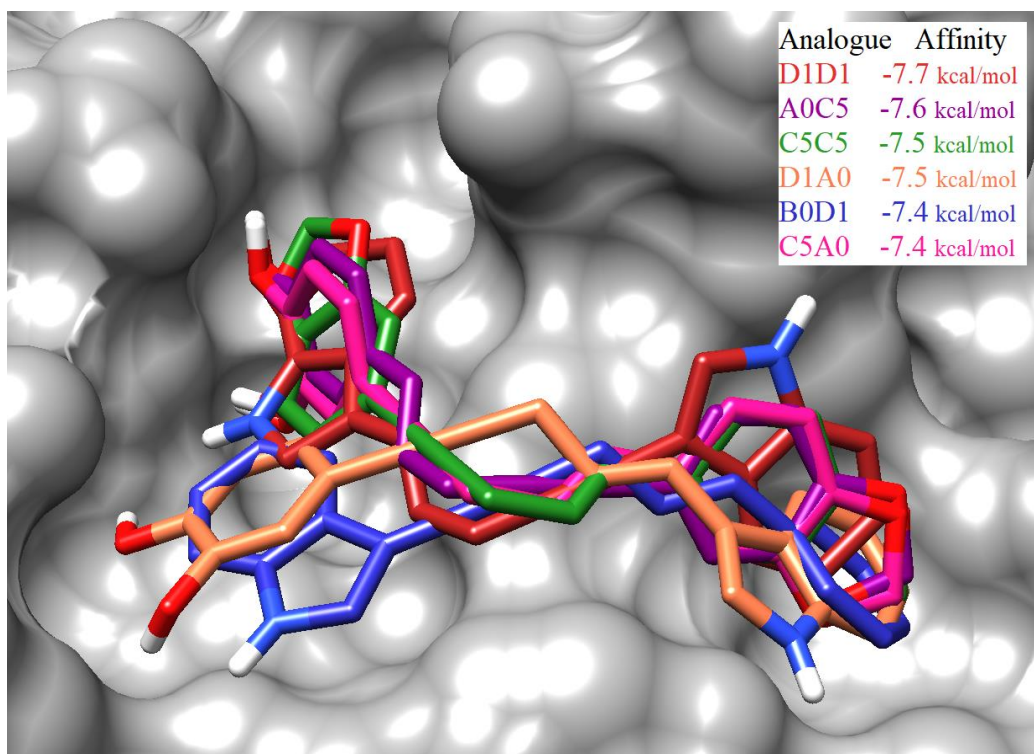


**Figure 21. Highest predicted binding energy rooperol analogues docked on 1LEW.** The top 6 highest binding energy scores were selected, and those poses shown in DRS pocket of p38 $\alpha$ . Each analogue carbon chain is differently colored as shown in table, and atoms of oxygen red, nitrogen blue and hydrogen white.

With first observation, all the highest binding energy analogues have an interaction at the  $\Phi_L$  pocket with the aromatic ring of the molecule centered above the pocket. Secondly, all analogues have an interaction with one of the two electrostatic pockets,  $\Psi_L$  or  $\Psi_U$ . Lastly, some of the analogues have an interaction with  $\Phi_U$  pocket, orienting the aromatic ring over the pocket. Focus was primarily given to the electrostatic sites, as they had the most variability between the analogues. After looking at the top six scoring analogues models D1D1, A0C5, C5C5, D1A0, B0D1, and C5A0, all of the models except one, B0D1, had a catechol within a close distance of an electrostatic

interaction with ARG 136 as seen in Figure 22. The exception, B0D1, had the aromatic ring of its indole group near ARG 136, and did not fit the trend. The next point of focus was the interaction with the two hydrophobic pockets,  $\Phi_U$  and  $\Phi_L$ . It was observed that analogues with greater binding energy interacted with both of the above pockets and oriented their aromatic rings towards these pockets.

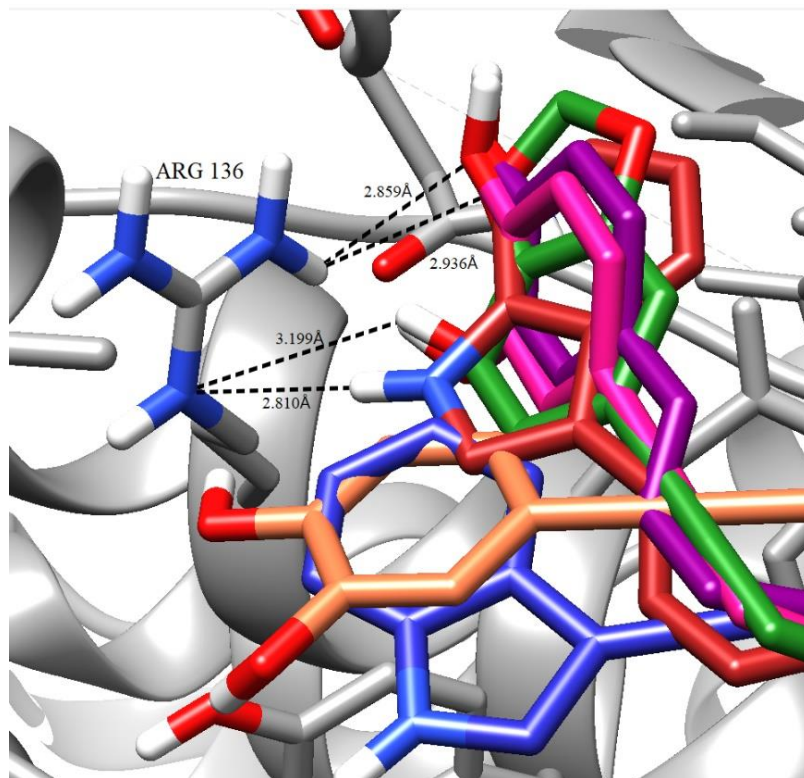


**Figure 22. Highest predicted binding energy rooperol analogues' interaction with ARG 136.** Top six highest predicted binding energy analogues shown in the left electrophilic  $\Psi_L$  and  $\Psi_U$  end of the pocket. Distances between ARG 136 and analogue atoms labeled.

To further understand analogues for potential ability to be used for anti-cancer therapy, an *in vitro* cell assay was done to measure  $IC_{50}$  values for rooperol and analogues. Five analogues and rooperol were tested by Du Lab Texas State University using a fluorescence cell survival assay as seen in Table 3.

**Table 3. Cytotoxicity and highest predicted affinity data of tested rooperol and analogues.** Cytotoxicity data provided by Du Lab at Texas State, docking results acquired using AutoDock Vina.

Compound	IC <sub>50</sub> HeLa cells ( $\mu$ M)	Affinity (kcal/mol)
A0/A0	18 $\pm$ 3	-7.1
A1/A1	33.2 $\pm$ 0.7	-6.6
A4/A4	77 $\pm$ 10	-7.2
B4/B4	>500	-7.0
C5/C5	112 $\pm$ 3	-7.5
C5/A0	38 $\pm$ 8	-7.4

Initial observation of the predicted binding energy and cytotoxicity data shows that the two are not directly related. This may indicate that p38 $\alpha$  inhibition is not related to the mechanism of cytotoxicity against the HeLa cancer cell line. However, more definitive evidence for p38 $\alpha$ 's role, or lack thereof, in the anticancer effects of rooperol and analogs will require experimental evaluation of p38 $\alpha$  kinase inhibition and its possible correlation with the cytotoxicity of these analogues against an array of cancer cell lines.

Despite the overall lack of correlation between docking results and cytotoxicity for this limited set of compounds, there are two pairs of interesting results. The two compounds with lowest IC<sub>50</sub> values, A0A0 (rooperol) and A1A1, are near the mean and lower end of predicted binding energy data. Secondly the two compounds with high predicted binding affinities C5C5 and C5A0, display very different IC<sub>50</sub> values. Most clearly is that the B4B4 analogue, has the highest IC<sub>50</sub> value. Each of these analogues were compared with pose of highest analogue and IC<sub>50</sub> value. Initially the outlier, B4B4 binds pose binds in the  $\Psi_T$  and  $\Psi_L$  pockets seen in Figure 23.

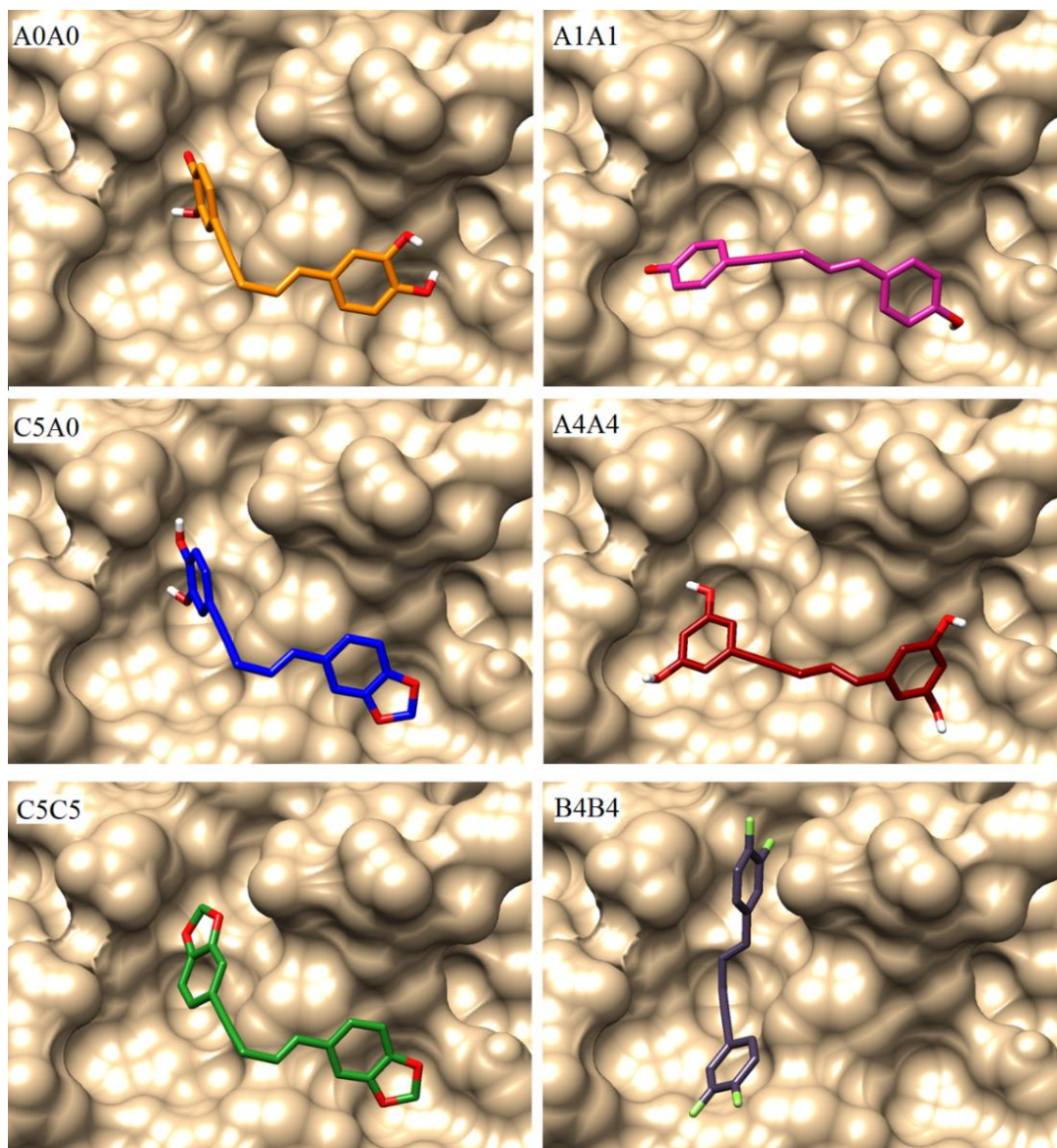


**Figure 23. Cytotoxicity tested rooperol analogues resulting pose within DRS pocket.** Selecting analogues tested in cell cytotoxicity assay, the highest predicted binding energy pose docked into p38 $\alpha$  shown.

After seeing B4B4 as the outlier, further analysis focused on  $\Psi$  pocket interactions, and the results showed an increase in electrostatic interactions to ARG 136 over the various analogues as seen in Figure 24.

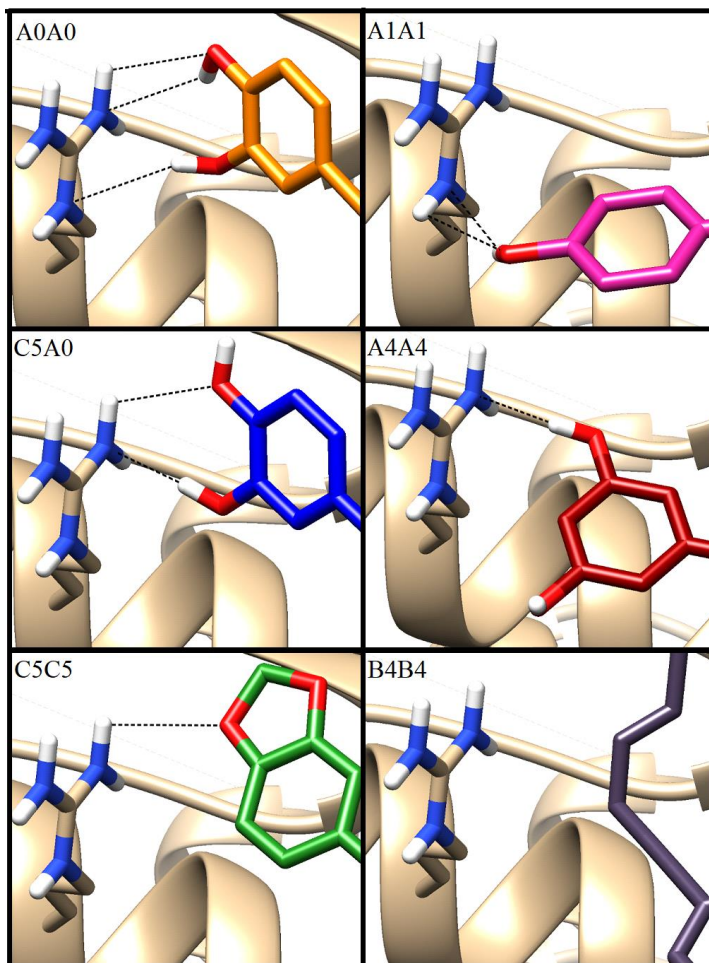


**Figure 24. Cytotoxicity tested rooperol analogues pose interaction with ARG 136.** The results of docking studies onto p38 $\alpha$  of those analogues tested for cytotoxicity. Atoms in analogues and ARG 136 are shown colored by heteroatom, nitrogen atoms colored blue, oxygen colored red and hydrogen white. Each analogue has carbons colored varied.

While this gave an initial correlation to cytotoxicity results, it did not fully describe the interaction with the DRS, or mechanism of cytotoxicity. With the previous work on pockets, it is believed the combination of more electrostatic interactions, positioning to block both pockets  $\Phi_U$  and  $\Phi_L$  better captures the DRS binding energy and inhibition. Through the poses of the various analogues and a clearer picture of the binding interaction on p38 $\alpha$ , a more focused approach can be taken for synthesis of analogues which can achieve interaction at these points and possibly increase inhibition.

## IV. CONCLUSION

The goal of this project was to characterize the inhibition of p38 $\alpha$  by rooperol and rooperol analogues, and to identify analogues with greater inhibition for further potential use. We discovered through an ELISA and ADP-Glo techniques that the measurement of p38 $\alpha$  activity was better identified by measuring the production of ADP rather than phosphorylated protein due to antibody non-specific binding issues. Initial *in vitro* work with the ADP-Glo™ technique made strides in honing the ADP Percent Conversion curve, and initial enzyme concentrations, for measurement of kinase activity and was handed off to be further improved. Molecular docking was done and found interesting results, including the specificity of DRS pocket interactions that are influenced by protein binding direction, selectivity of rooperol pocket binding due to ligand direction, and cytotoxicity and rooperol orientation relationships which could provide insight onto specific pocket binding interactions.

### **p38 $\alpha$ DRS pocket structure**

The results from docking rooperol in ATP binding and the DRS site showed a more favorable predicted binding energy for the DRS. Subsequent docking of rooperol to various p38 $\alpha$  structures at DRS found an importance on the direction of protein ligand binding in correlation to the affinities and poses of rooperol. The side of the pocket nearest to the *N*-terminus of the ligand had more pocket accessibility and rooperol bound more readily to the space. The key interactions were identified as ARG 136, near the two electrophilic pockets, and the occupation of both hydrophobic  $\Phi_U$  and  $\Phi_L$  pockets. Lastly, binding with non-ligand bound protein crystal structures showed continued influence of the accessibility of pockets. Lastly, the structure bound to SB203580 an ADP inhibitor,

found an increase binding energy as compared to other dockings, noting the cross-talk affect observed in *in vitro* studies in Li *et al.*<sup>19</sup>.

### **p38 $\alpha$ and rooperol analogues**

Overall docking of rooperol analogues showed that those analogues greater binding energy had interactions with  $\Phi_U$  and  $\Phi_L$  pockets, and one of the two electrophilic pockets. Furthermore, the analogue with the highest predicted binding energy, D1D1 interacted with  $\Psi_L$ ,  $\Phi_U$ , and  $\Phi_L$ . In addition to the pockets, the occupation of the space between the two hydrophobic pockets  $\Phi_U$ , and  $\Phi_L$ , and electrophilic interactions with ARG136 and ASP 161 were noted for possible key interactions for specific binding.

### **p38 $\alpha$ and cytotoxicity tested rooperol analogues**

Results of cytotoxicity testing with various analogues did not correlate to predicted affinities. Upon observation of binding poses of cytotoxic analogues, the binding within the  $\Psi_L$  site with the greater interaction with ARG 136, showed similar ranking but did not fully encompass the interaction with additional contributions of binding of the  $\Phi_U$ , and  $\Phi_L$  pockets but further work still must be done to understand cytotoxicity.

### **Future work**

In continuation of this project, further docking studies using a dynamic program which could simulate dynamic docking, in addition to further *in vitro* testing of analogues with use of the ADP-Glo™ assay can be done.

## APPENDIX SECTION

	<b>Page</b>
<b>D-Recognition Site Pocket Structure</b>	
Figure 1A. DRS of 1LEW .....	46
Figure 2A. Sequence Alignment of p38 $\alpha$ in mouse and human .....	47
Figure 3A. Sequence Alignment of p38 $\alpha$ in various organisms .....	48
Figure 4A. Pocket Shape Variation Due to Peptide Binding Direction.....	49
<b>Docking Analogue Results</b>	
Figure 5A. A0A analogues .....	50
Figure 6A. A0B analogues.....	51
Figure 7A. A0C and A0D analogues .....	51
Figure 8A. A1 analogues .....	52
Figure 9A. A2 analogues .....	52
Figure 10A. A3 analogues .....	53
Figure 11A. A4 analogues .....	53
Figure 12A. B0A analogues.....	54
Figure 13A. B0B analogues.....	54
Figure 14A. B0C and B0D analogues.....	55
Figure 15A. B1 analogues.....	55
Figure 16A. B2 analogues.....	56
Figure 17A. B3 analogues.....	56
Figure 18A. B4 analogues.....	57
Figure 19A. C2 analogues.....	57
Figure 20A. C3 analogues.....	58
Figure 21A. C4 analogues.....	58
Figure 22A. C5 analogues.....	59
Figure 23A. D1 analogues .....	59

## D - Recognition Site pocket structure

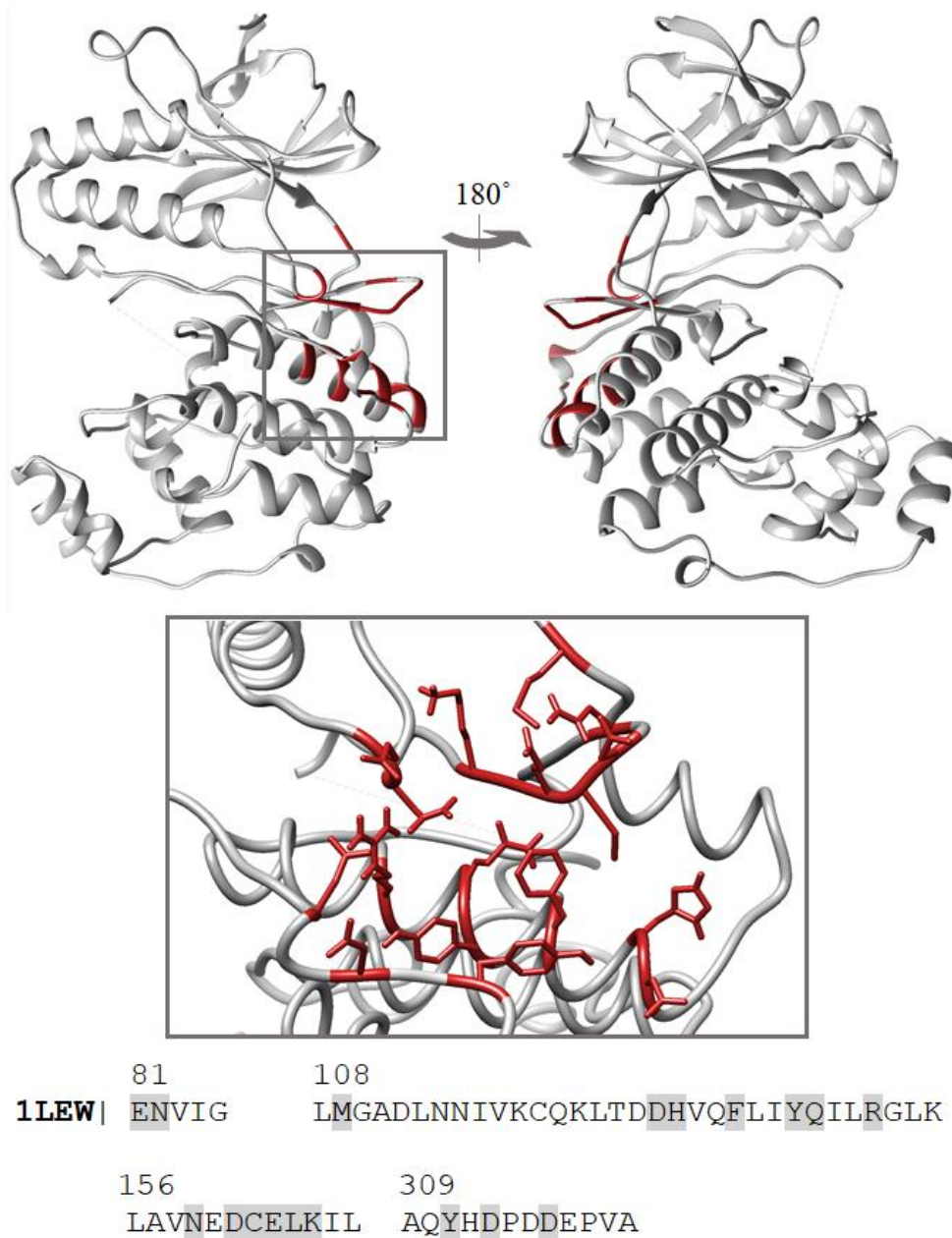


**Figure 1A. DRS of 1LEW.** The location of the DRS on 1LEW, the full structure of p38 $\alpha$  with DRS colored red and boxed, that box expanded, with those residues below highlighted in the sequence.

```

SP|Q16539|MK14_HUMAN MSQERPTFYRQELNKTIWEVPERYQNLSPVSGAYGSVCAAFDTKTGLRVAVKKLSRPFQ 60
SP|P47811|MK14_MOUSE MSQERPTFYRQELNKTIWEVPERYQNLSPVSGAYGSVCAAFDTKGHRVAVKKLSRPFQ 60
*****

SP|Q16539|MK14_HUMAN SIIHAKRTYRELRLKMKHENVIGLLDVFTPARSLEEFNDVYLVTHLMGADLNNIVKCQ 120
SP|P47811|MK14_MOUSE SIIHAKRTYRELRLKMKHENVIGLLDVFTPARSLEEFNDVYLVTHLMGADLNNIVKCQ 120
*****

SP|Q16539|MK14_HUMAN KLTDDHVQFLIYQILRGLKYIHSADIIHRDLKPSNLAVNEDCELIKILDFGLARHTDEMT 180
SP|P47811|MK14_MOUSE KLTDDHVQFLIYQILRGLKYIHSADIIHRDLKPSNLAVNEDCELIKILDFGLARHTDEMT 180
*****

SP|Q16539|MK14_HUMAN GYVATRWRAP EIMLNWMHYNQTVDIWSVGCIMAELLTGRTLFPGTDHIDQLKLILRLVG 240
SP|P47811|MK14_MOUSE GYVATRWRAP EIMLNWMHYNQTVDIWSVGCIMAELLTGRTLFPGTDHIDQLKLILRLVG 240
*****

SP|Q16539|MK14_HUMAN TPGAELLKKISSESARNYIQSLTQMPKMN FANVFIGANPLAVD LLEKMLVLDS DKRITAA 300
SP|P47811|MK14_MOUSE TPGAELLKKISSESARNYIQSLAQM PKMNFANVFIGANPLAVD LLEKMLVLDS DKRITAA 300
*****

SP|Q16539|MK14_HUMAN QALAHAYFAQYHDPDDEPVADPYDQSFESRDLLIDEWKSLTYDEVISFVPPPLDQEEMES 360
SP|P47811|MK14_MOUSE QALAHAYFAQYHDPDDEPVADPYDQSFESRDLLIDEWKSLTYDEVISFVPPPLDQEEMES 360
*****

```

**Figure 2A. Sequence Alignment of p38 $\alpha$  in mouse and human.** The p38 $\alpha$  sequence of human and mouse noting only three residues vary between the sequence outside of DRS



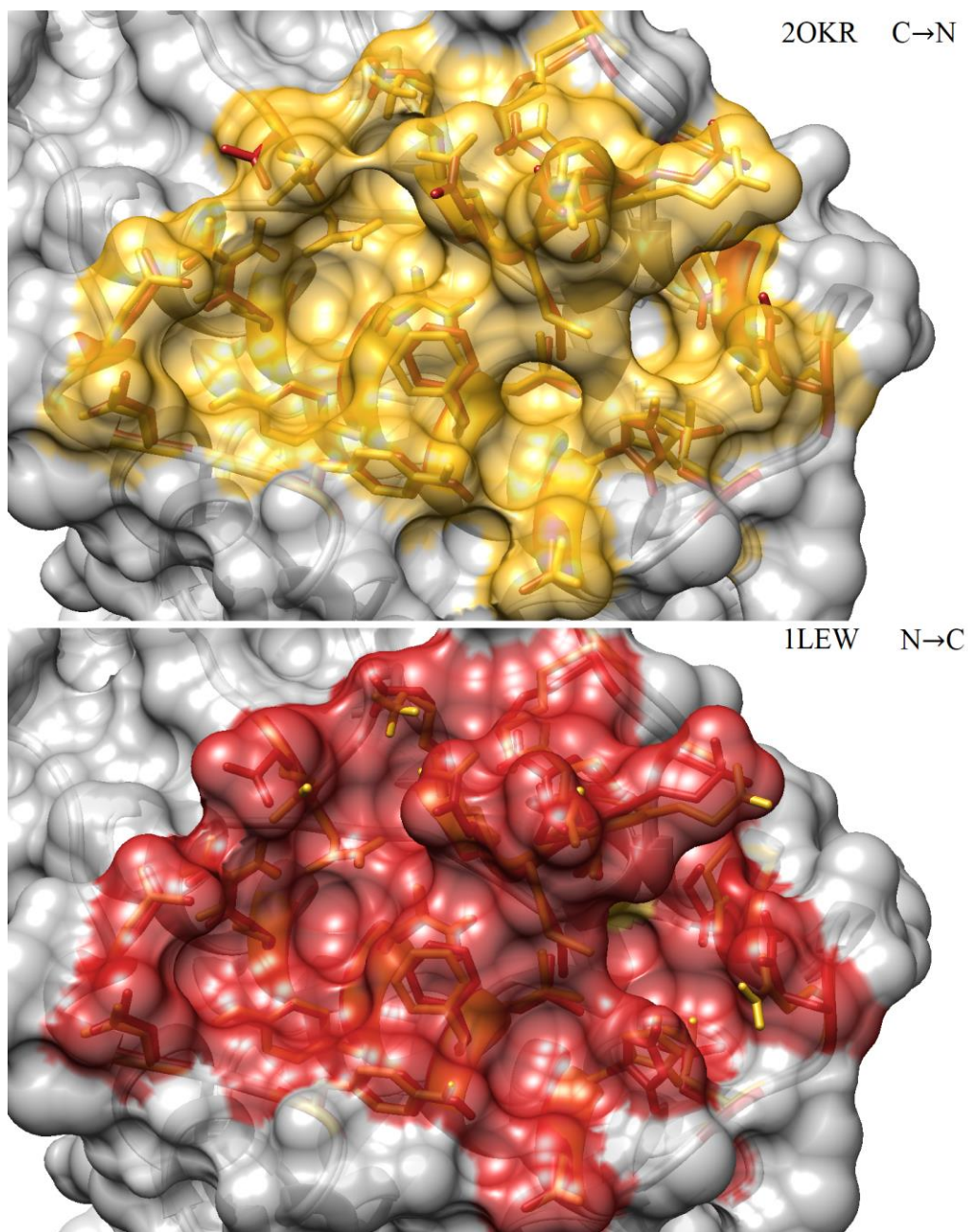


**Figure 4A. Pocket Shape Variation Due to Peptide Binding Direction.** An image of two examples of DRS pocket variation due to binding direction, above the C to N binder noting the shifting of residues below the  $\Psi_T$  pocket which close and create a bridge like closure of the pocket. Both protein structures, 1LEW and 2OKR have residues shown as sticks, but only a single surface is shown in each image.

## Rooperol Analogues Docking Results

The results of docking analogues grouped by initial alkene-proximal catechol, then alkyne-proximal catechol. Only the highest binding energy (found in table as affinity) predicted pose for each analogue depicted, created with Chimera opening the results from AutoDock Vina.

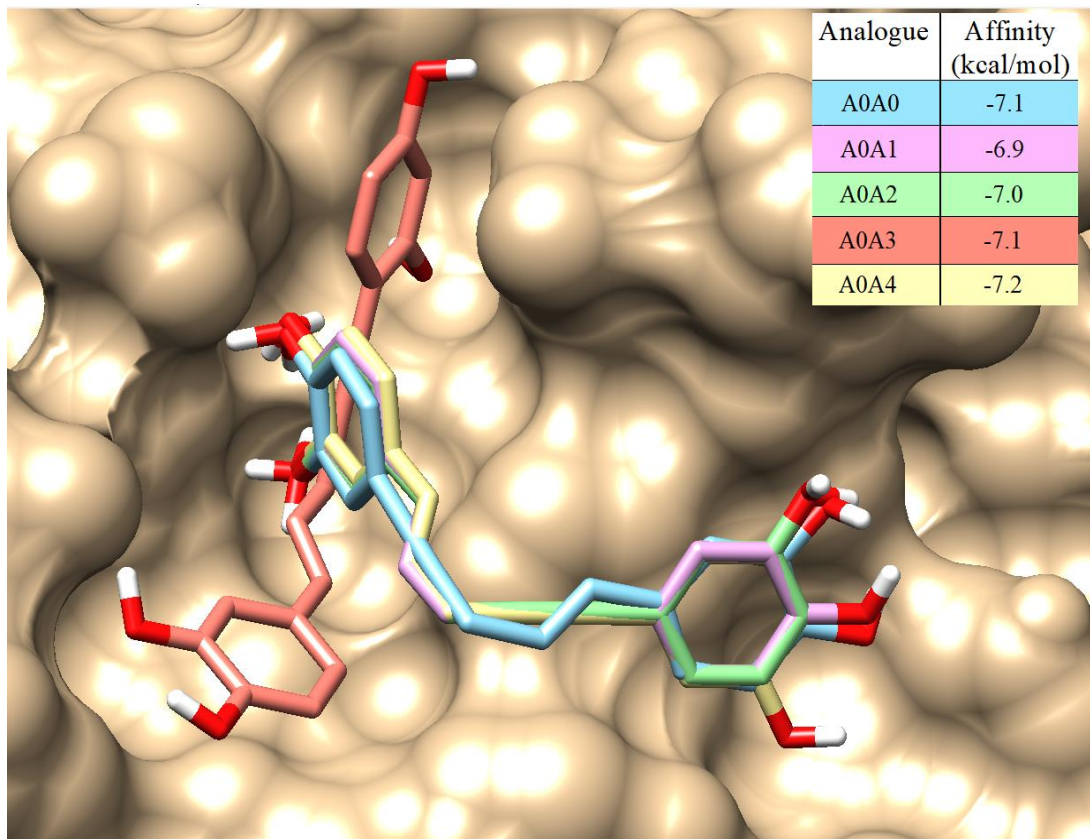
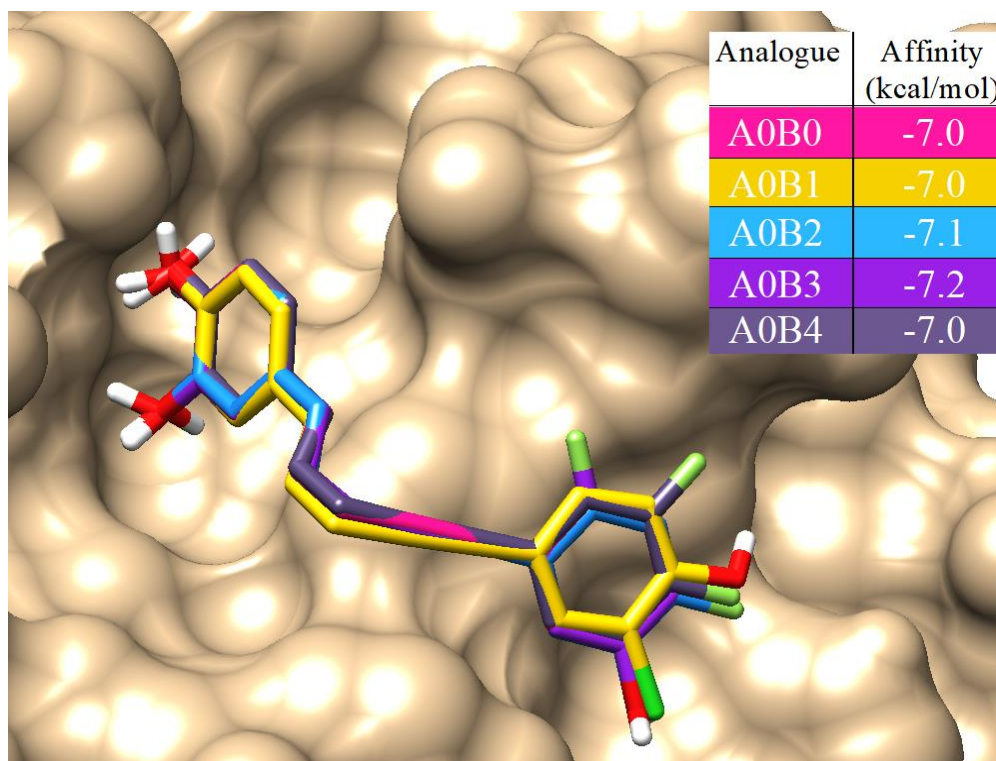
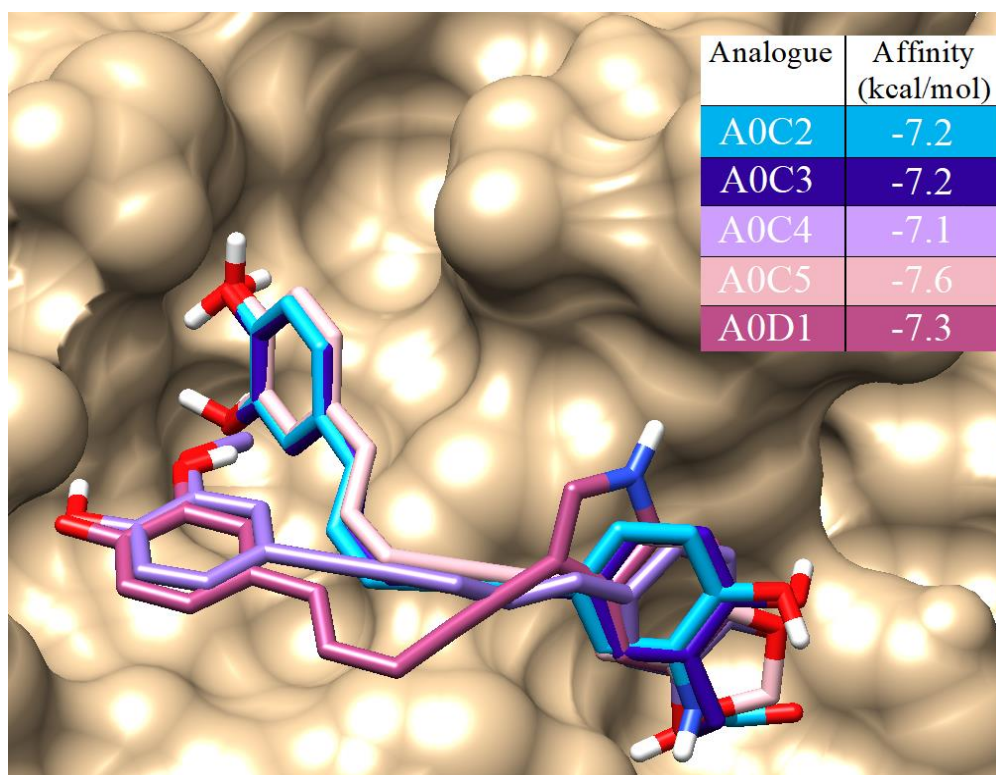


Figure 5A. A0A analogues



**Figure 6A. A0B analogues**



**Figure 7A. A0C and A0D analogues**

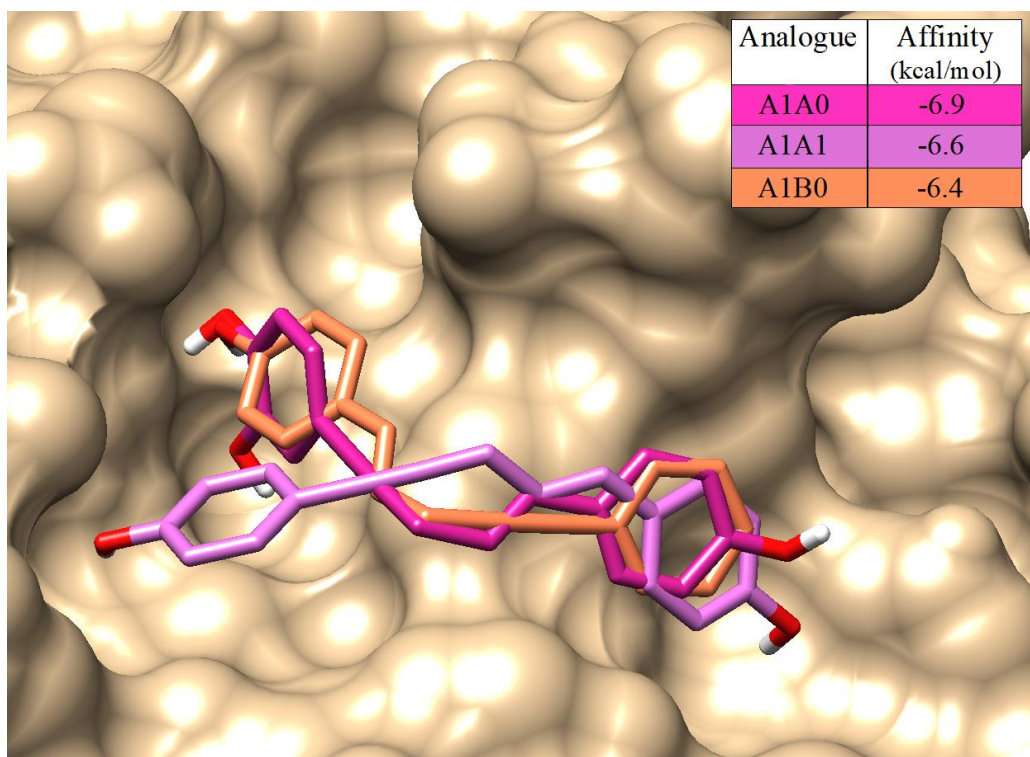


**Figure 8A. A1 analogues**

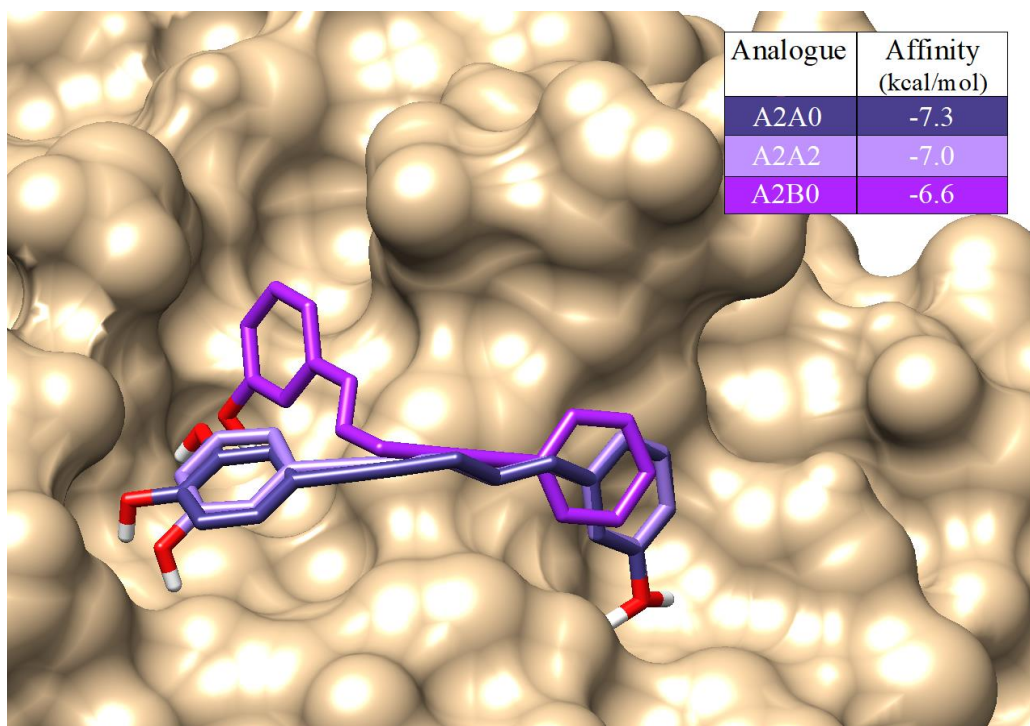


**Figure 9A. A2 analogues**

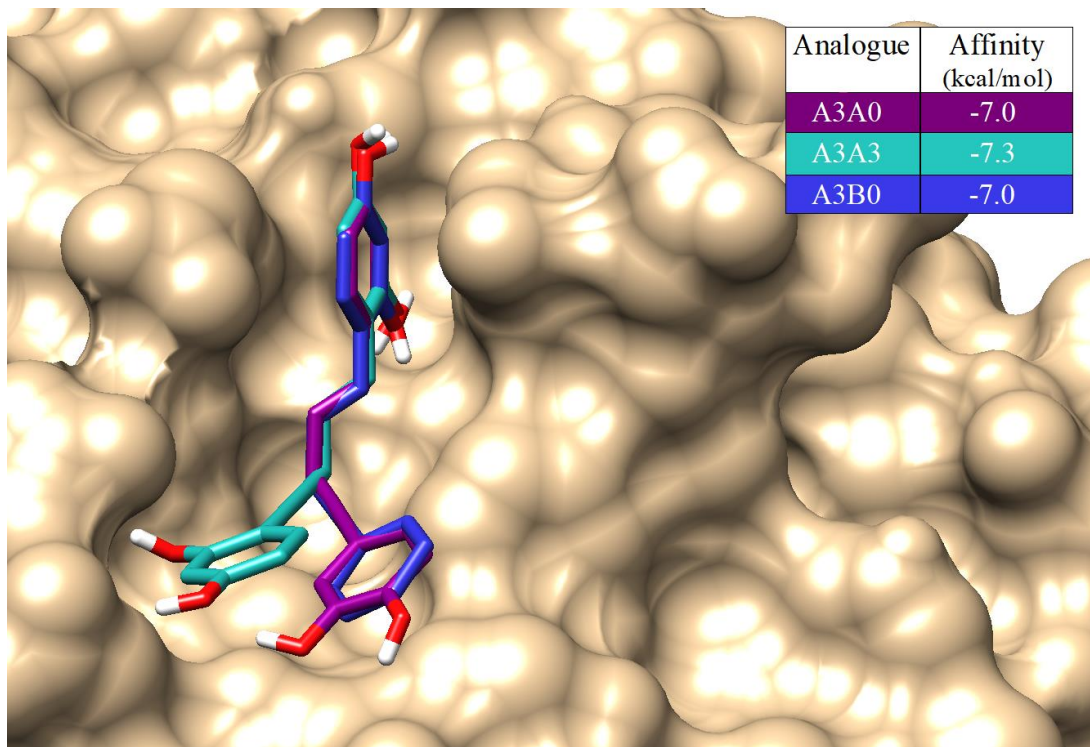


**Figure 10A. A3 analogues**

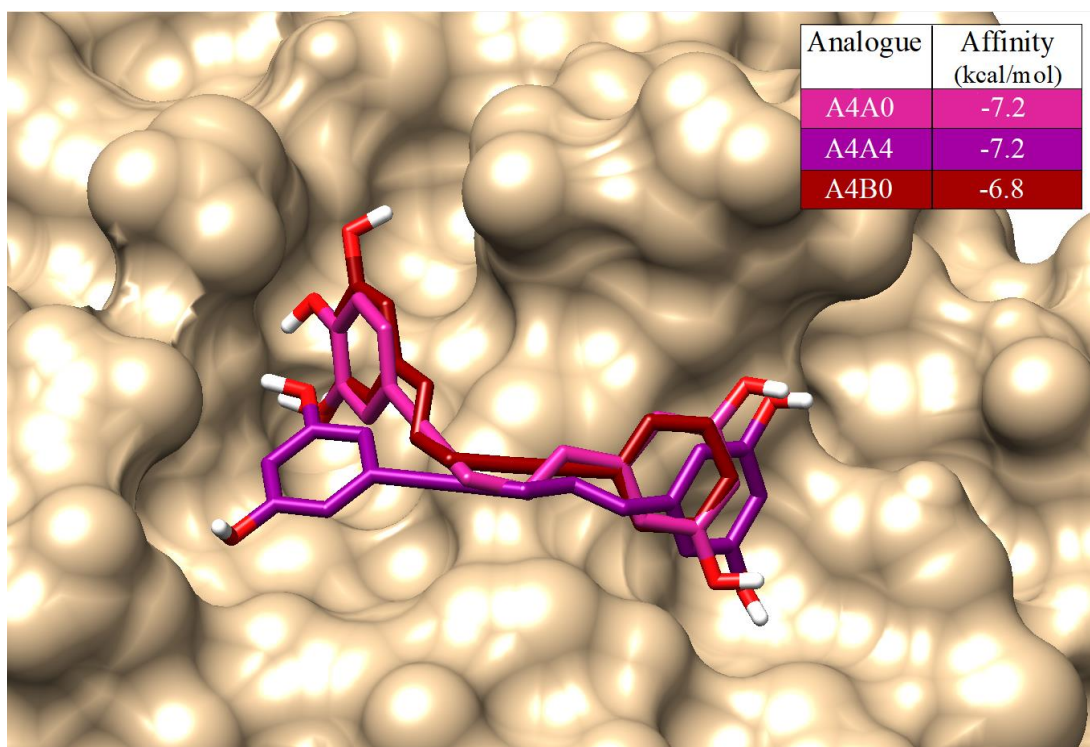


**Figure 11A. A4 analogues**

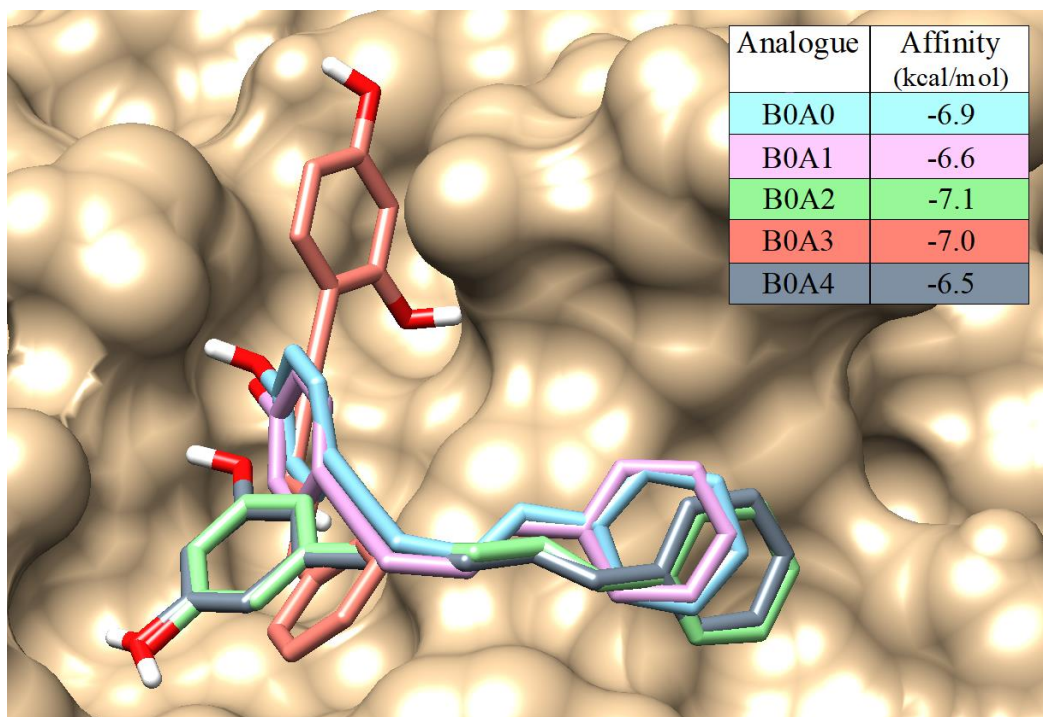


**Figure 12A. B0A analogues**

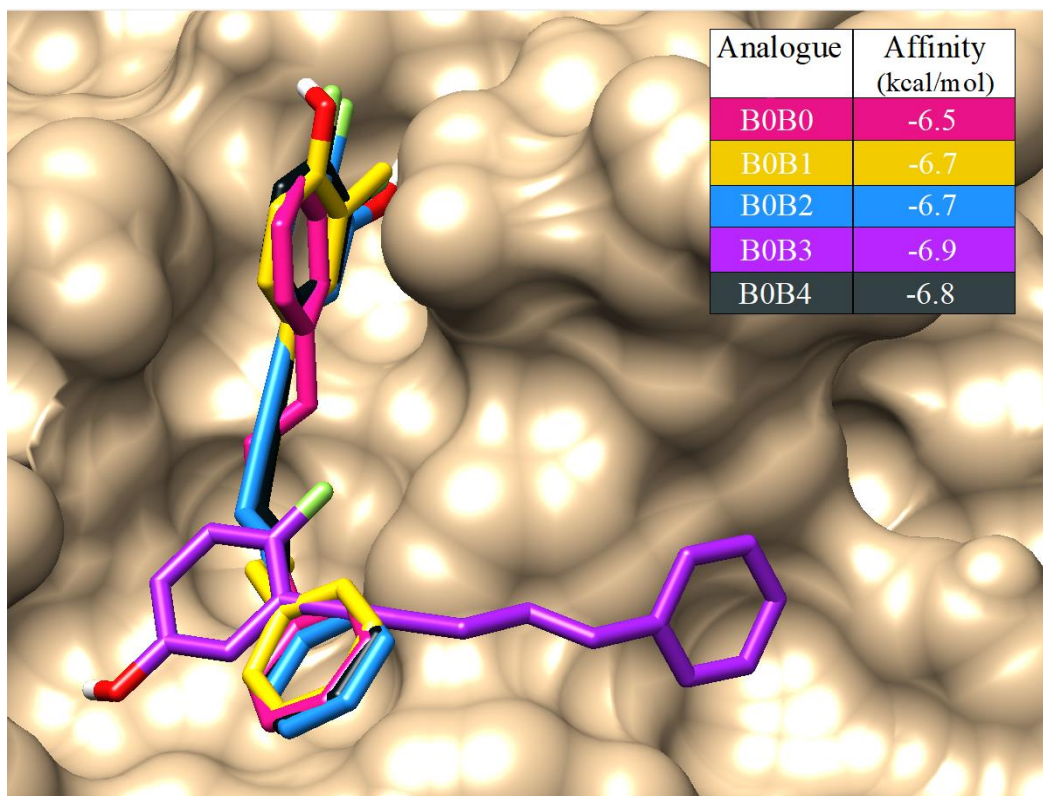


**Figure 13A. B0B analogues**

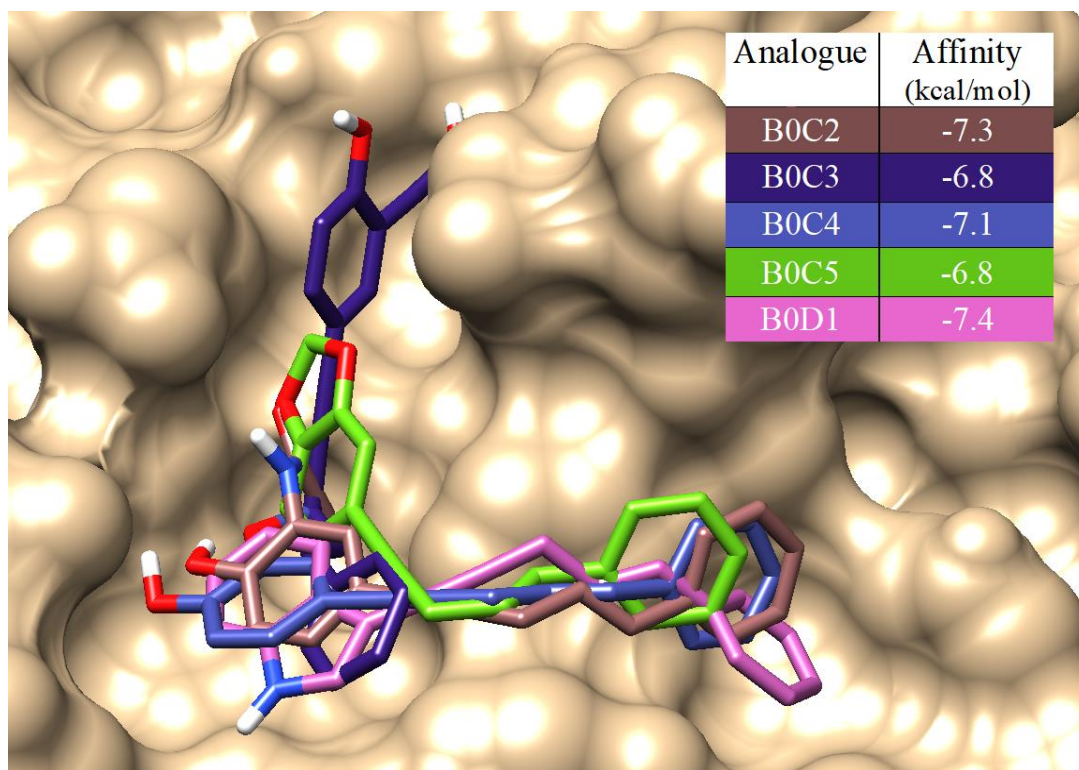


**Figure 14A. B0C and B0D analogues**

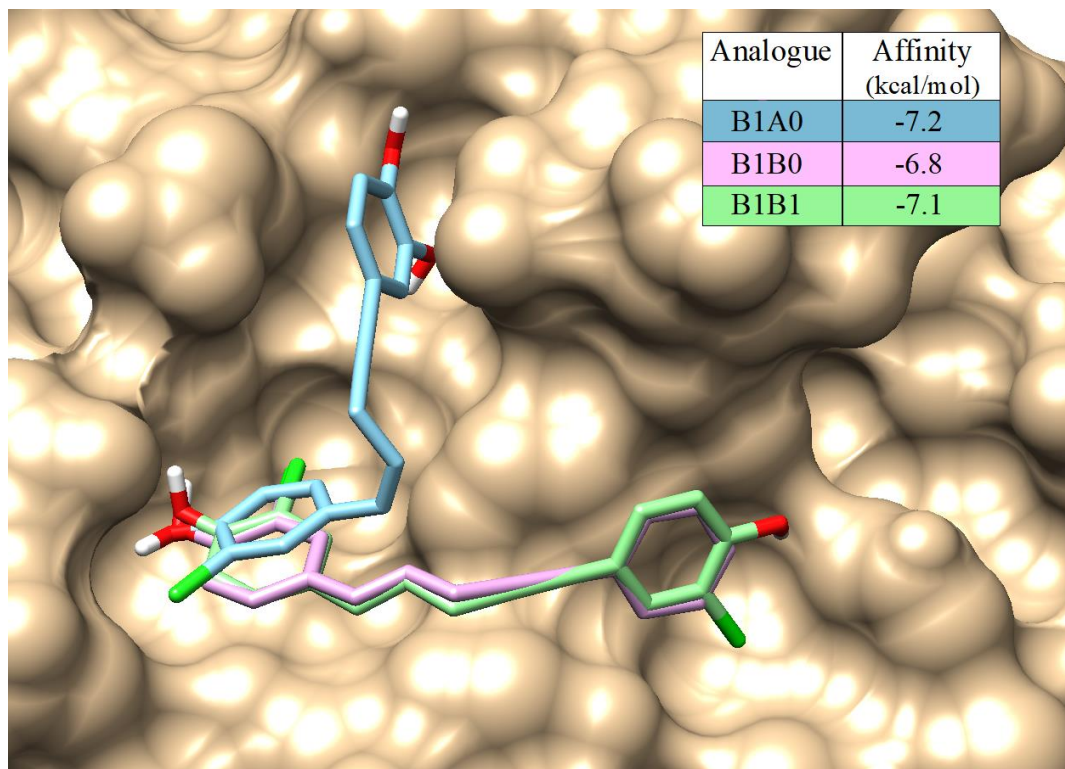


**Figure 15A. B1 analogues**

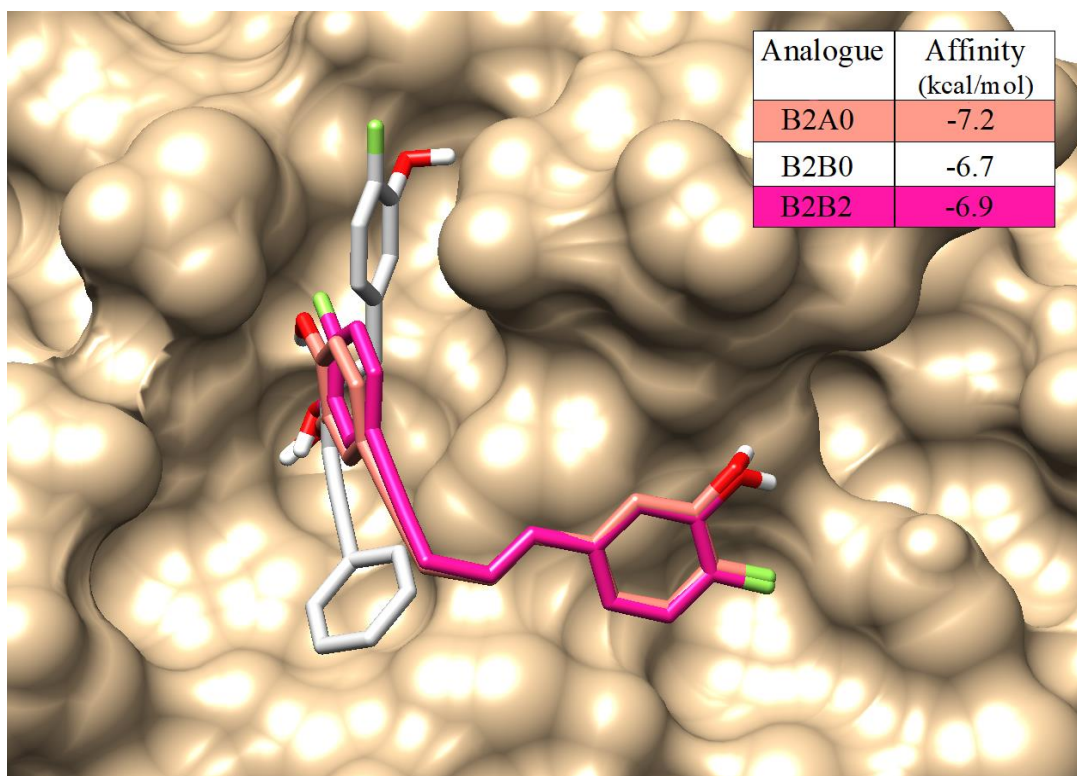


**Figure 16A. B2 analogues**

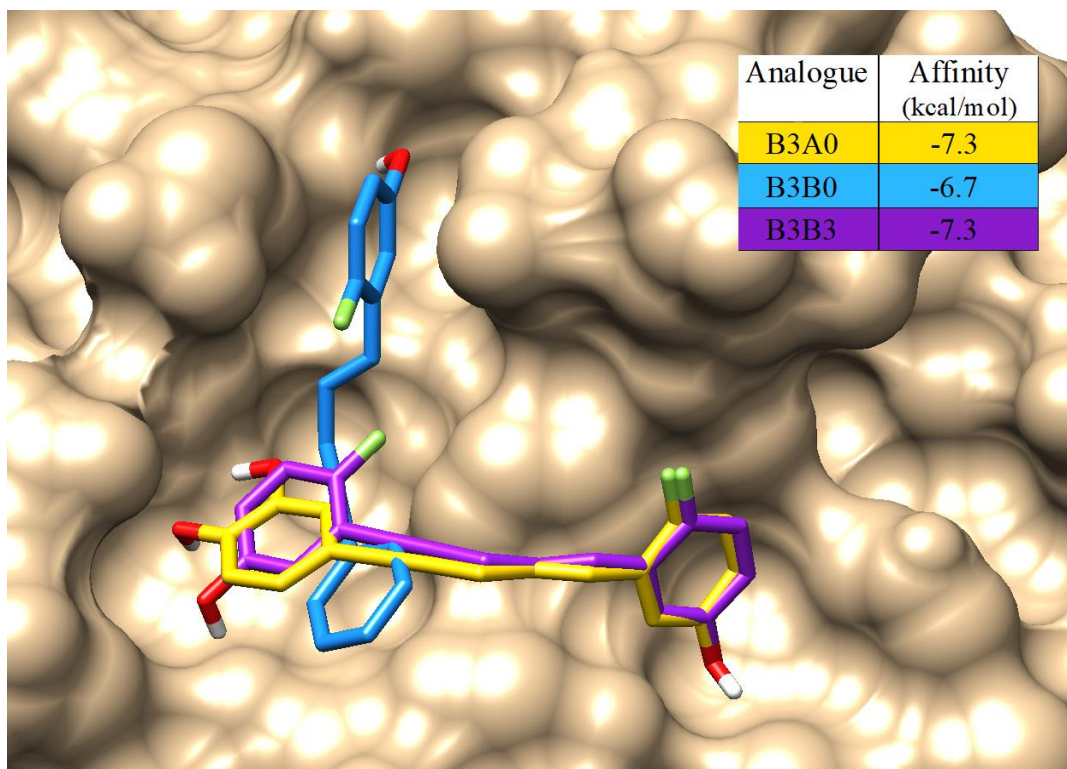


**Figure 17A. B3 analogues**

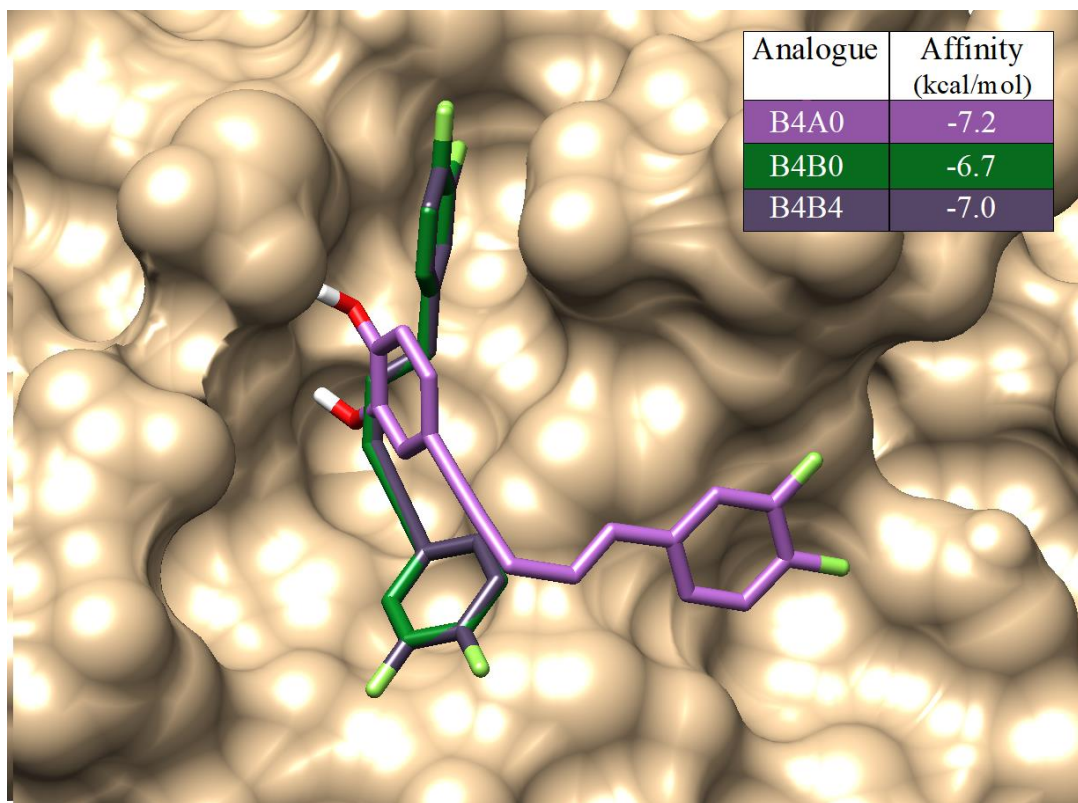


**Figure 18A. B4 analogues**

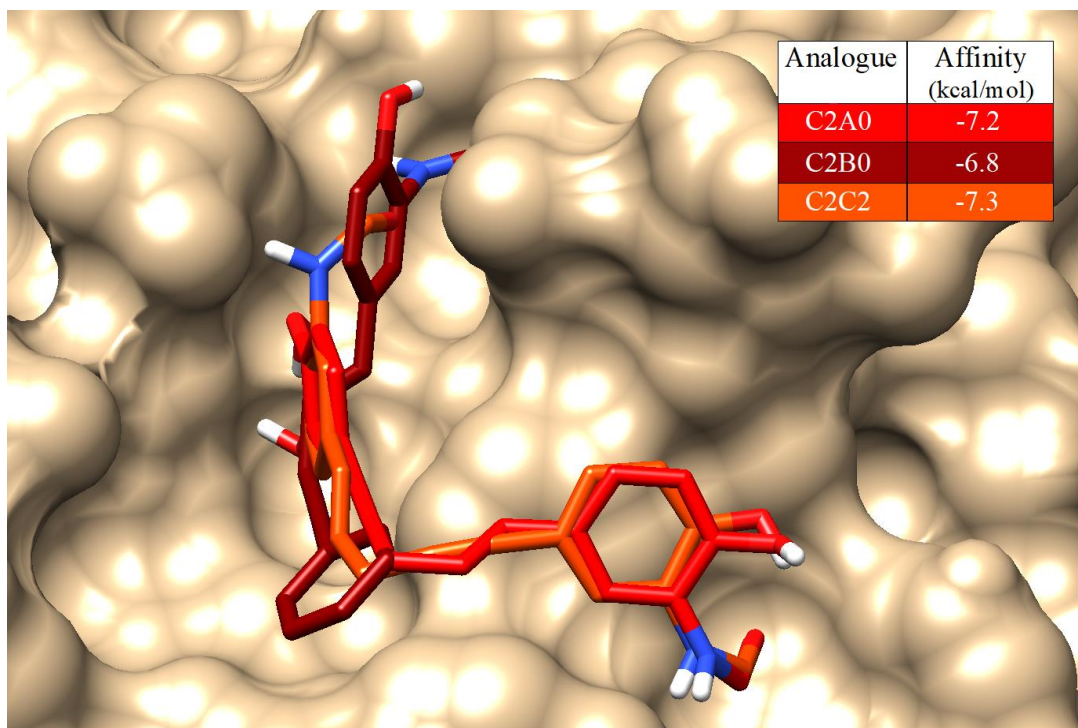


**Figure 19A. C2 analogues**

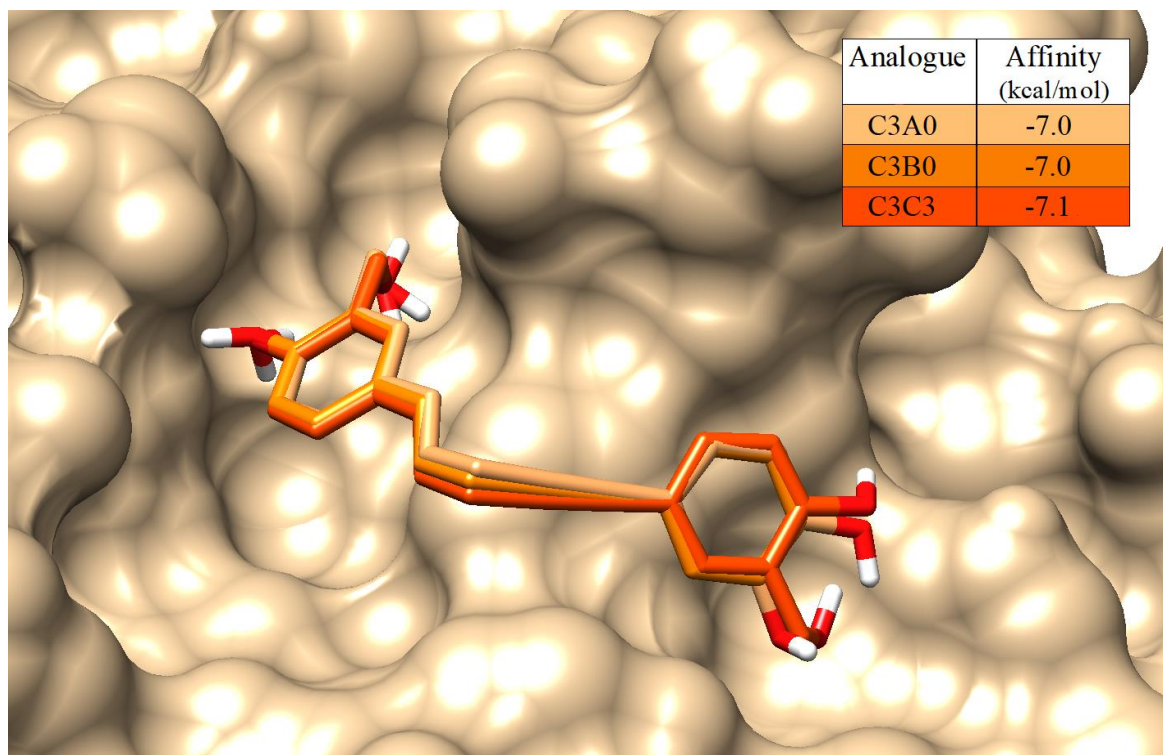


**Figure 20A. C3 analogues**

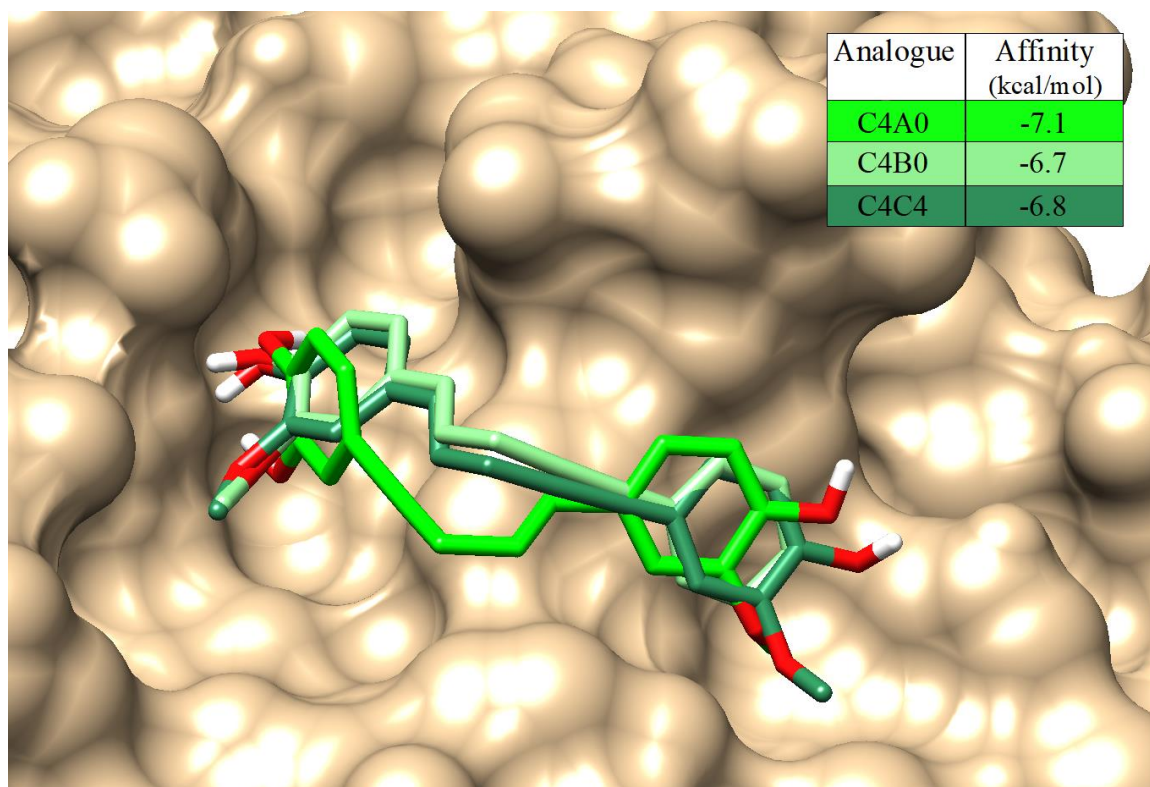


**Figure 21A. C4 analogues**

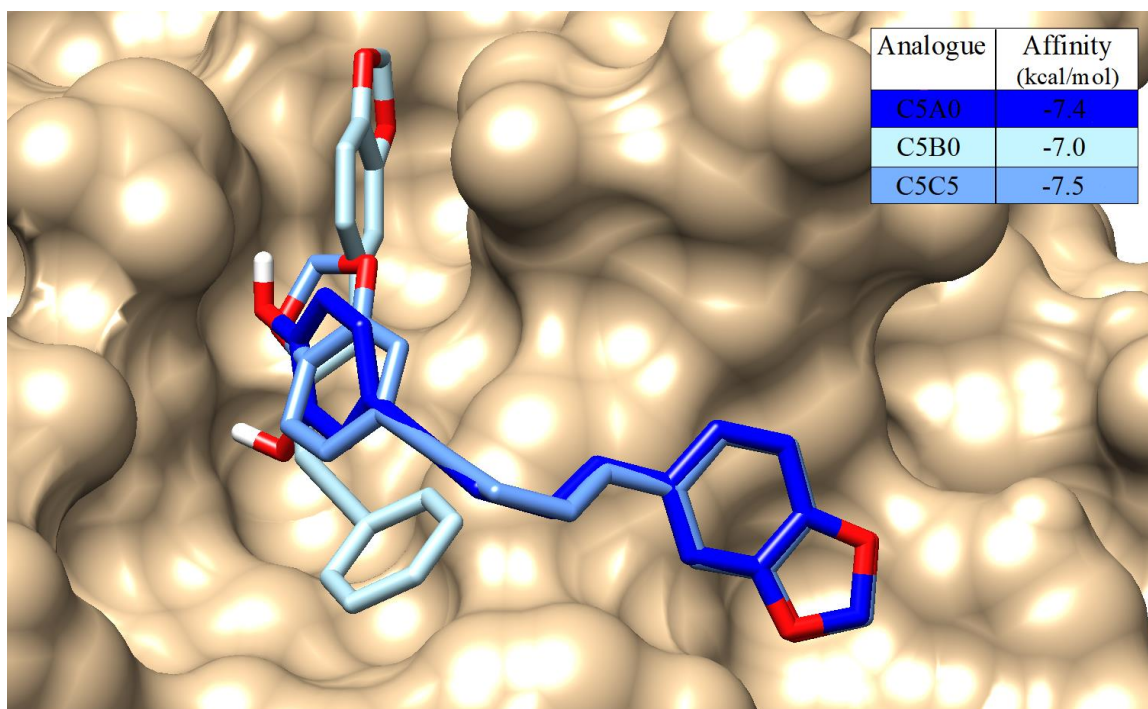


**Figure 22A. C5 analogues**

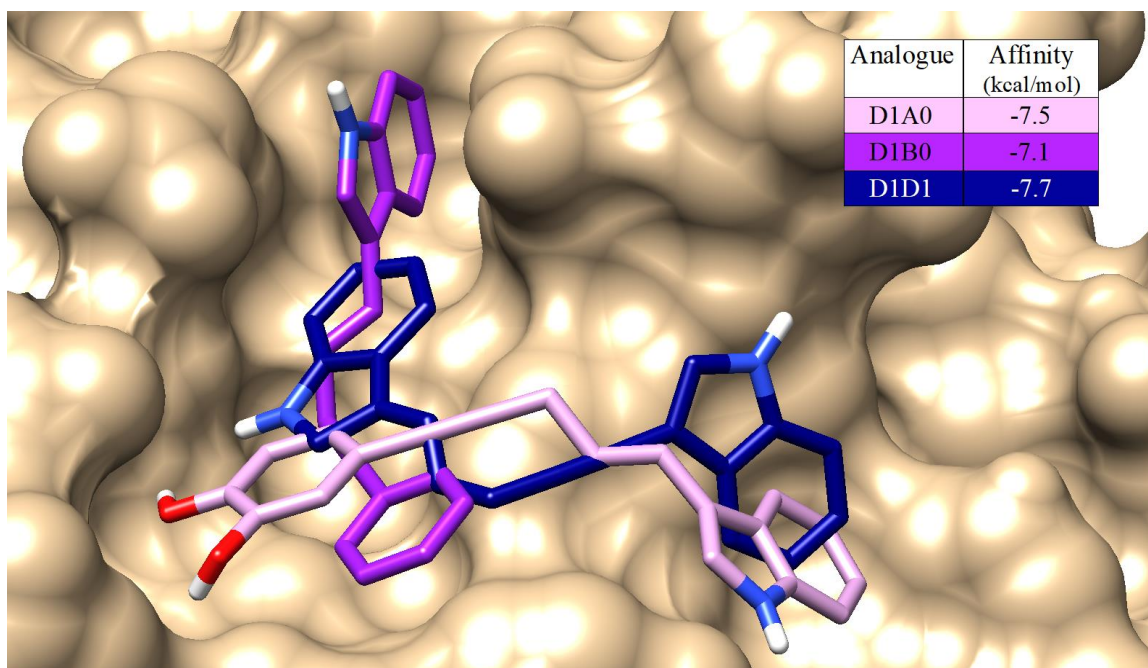


**Figure 23A. D1 analogues**

## LITERATURE CITED

1. Papac, R. J., Origins of cancer therapy. *Yale J Biol Med* **2001**, 74 (6), 391-8.
2. Demain, A. L.; Vaishnav, P., Natural products for cancer chemotherapy. *Microb. Biotechnol.* **2011**, 4 (6), 687-699.
3. Pagare, S., et al., Secondary Metabolites of Plants and their Role: Overview. *Curr.Trends Biotechnol. Pharm.* **2015**, 9 (3), 293-304.
4. War, A. R., et al., Mechanisms of plant defense against insect herbivores. *Plant Signal. Behav.* **2012**, 7 (10), 1306-1320.
5. Newman, D. J.; Cragg, G. M., Natural Products as Sources of New Drugs from 1981 to 2014. *J. Nat. Prod.* **2016**, 79 (3), 629-661.
6. Seca, A. M. L.; Pinto, D. C. G. A., Plant Secondary Metabolites as Anticancer Agents: Successes in Clinical Trials and Therapeutic Application. *Int. J. Mol. Sci.* **2018**, 19 (1), 263.
7. Robertson, J., et al., Essential medicines for cancer: WHO recommendations and national priorities. *Bull. World Health Organ.* **2016**, 94 (10), 735-742.
8. Chabner, B. A.; Roberts Jr, T. G., Chemotherapy and the war on cancer. *Nat. Rev. Cancer* **2005**, 5, 65.
9. Gerrits, C. J., et al., Topoisomerase I inhibitors: the relevance of prolonged exposure for present clinical development. *Br. J. Cancer* **1997**, 76 (7), 952-962.
10. Mansoori, B., et al., The Different Mechanisms of Cancer Drug Resistance: A Brief Review. *Adv. Pharm. Bull.* **2017**, 7 (3), 339-348.
11. Ncube, B., et al., Hypoxis (Hypoxidaceae) in African traditional medicine. *J. Ethnopharmacol.* **2013**, 150 (3), 818-827.
12. Drewes, S. E., et al., Isolation of hypoxoside from hypoxis rooperi and synthesis of (E)-1,5-bis(3',4'-dimethoxyphenyl)pent-4-en-1-yne. *Phytochemistry* **1984**, 23 (6), 1313-1316.
13. Mulholland, D. A.; Drewes, S. E., Global phytochemistry: indigenous medicinal chemistry on track in southern Africa. *Phytochemistry* **2004**, 65 (7), 769-782.
14. Boukes, G.; Van de Venter, M., *Cytotoxicity and mechanism(S) of action of Hypoxis spp. (African Potato) against HeLa, HT-29 and MCF-7 cancer cell lines.* 2011; Vol. 5, p 2766-2774.
15. Smit, B. J., et al., A phase I trial of hypoxoside as an oral prodrug for cancer therapy - absence of toxicity. . *S Afr Med* **1995**, 85 (9), 865-868.

16. Albrecht, C. F., et al., Morphological characterisation of the cell-growth inhibitory activity of rooperol and pharmacokinetic aspects of hypoxoside as an oral prodrug for cancer therapy. *S Afr Med J* **1995**, 85 (9), 853-60.
17. Theron, E. J., et al., beta-Glucosidase activity in fetal bovine serum renders the plant glucoside, hypoxoside, cytotoxic toward B16-F10-BL-6 mouse melanoma cells. *In Vitro Cell Dev Biol Anim* **1994**, 30a (2), 115-9.
18. Ali Azouaou, S., et al., Selective ROS-dependent p53-associated anticancer effects of the hypoxoside derivative rooperol on human teratocarcinoma cancer stem-like cells. *Invest New Drugs* **2015**, 33 (1), 64-74.
19. Li, J., et al., A fluorescence-based assay for p38alpha recruitment site binders: identification of rooperol as a novel p38alpha kinase inhibitor. *ChemBioChem* **2013**, 14 (1), 66-71.
20. Porras, A.; Guerrero, C., Role of p38 $\alpha$  in apoptosis: implication in cancer development and therapy. *Atlas Genet Cytogenet Oncol Haematol.* **2011**, 15 (3), 316-326.
21. Avruch, J., MAP kinase pathways: the first twenty years. *Biochim Biophys Acta* **2007**, 1773 (8), 1150-60.
22. Goldsmith, E. J., et al., Substrate and docking interactions in serine/threonine protein kinases. *Chem Rev* **2007**, 107 (11), 5065-81.
23. Gomez-Gutierrez, P., et al., Identification of Potential Small Molecule Binding Pockets in p38alpha MAP Kinase. *J Chem Inf Model* **2017**, 57 (10), 2566-2574.
24. Chang, C. I., et al., Crystal structures of MAP kinase p38 complexed to the docking sites on its nuclear substrate MEF2A and activator MKK3b. *Mol Cell* **2002**, 9 (6), 1241-9.
25. Cuenda, A.; Rousseau, S., p38 MAP-kinases pathway regulation, function and role in human diseases. *Biochim Biophys Acta* **2007**, 1773 (8), 1358-75.
26. Bradham, C.; McClay, D. R., p38 MAPK in Development and Cancer. *Cell Cycle* **2006**, 5 (8), 824-828.
27. Ono, K.; Han, J., The p38 signal transduction pathway Activation and function. *Cell. Signalling* **2000**, 12 (1), 1-13.
28. Pearson, G., et al., Mitogen-activated protein (MAP) kinase pathways: regulation and physiological functions. *Endocr Rev* **2001**, 22 (2), 153-83.
29. Reményi, A., et al., Docking interactions in protein kinase and phosphatase networks. *Curr. Opin. Struct. Biol.* **2006**, 16 (6), 676-685.

30. Breitwieser, W., et al., Feedback regulation of p38 activity via ATF2 is essential for survival of embryonic liver cells. *Genes Dev.* **2007**, *21* (16), 2069-2082.
31. Boldt, S., et al., The role of MAPK pathways in the action of chemotherapeutic drugs. *Carcinogenesis* **2002**, *23* (11), 1831-8.
32. Lau, E.; Ronai, Z. e. A., ATF2 – at the crossroad of nuclear and cytosolic functions. **2012**, *125* (12), 2815-2824.
33. Kerwin, S. M.; Cha, J., A concise synthesis of rooperol and related 1,5-diarylpent-1-en-4-yne. *Tetrahedron Lett.* **2014**, *55* (1), 137-141.
34. Peti, W.; Page, R., Molecular basis of MAP kinase regulation. *Protein Science* **2013**, *22* (12), 1698-710.
35. Shah, N. G., et al., Novel Noncatalytic Substrate-Selective p38alpha-Specific MAPK Inhibitors with Endothelial-Stabilizing and Anti-Inflammatory Activity. *J Immunol* **2017**, *198* (8), 3296-3306.
36. Hendriks, B. S., et al., Two additive mechanisms impair the differentiation of 'substrate-selective' p38 inhibitors from classical p38 inhibitors in vitro. *BMC Syst Biol* **2010**, *4*, 23.
37. Goettert, M., et al., Optimization of a nonradioactive immunosorbent assay for p38alpha mitogen-activated protein kinase activity. *Anal Biochem* **2010**, *406* (2), 233-4.
38. Bauer, S. M., et al., A direct enzyme-linked immunosorbent assay (ELISA) for the quantitative evaluation of Janus Kinase 3 (JAK3) inhibitors. *Anal. Methods* **2014**, *6* (21), 8817-8822.
39. Glickman, J. F., Assay Development for Protein Kinase Enzymes. In *Assay Guidance Manual*, Sittampalam, G. S., et al., Eds. Eli Lilly & Company and the National Center for Advancing Translational Sciences: Bethesda (MD), 2004.
40. Zegzouti, H., et al., ADP-Glo: A Bioluminescent and homogeneous ADP monitoring assay for kinases. *Assay Drug Dev Technol* **2009**, *7* (6), 560-72.
41. Garai, A., et al., Specificity of linear motifs that bind to a common mitogen-activated protein kinase docking groove. *Sci Signal* **2012**, *5* (245), ra74.
42. White, A., et al., Molecular basis of MAPK-activated protein kinase 2:p38 assembly. *Proc Natl Acad Sci U S A* **2007**, *104* (15), 6353-8.
43. ter Haar, E., et al., Crystal structure of the p38 alpha-MAPKAP kinase 2 heterodimer. *J Biol Chem* **2007**, *282* (13), 9733-9.

44. Honndorf, V. S., et al., Inferential NMR/X-ray-based structure determination of a dibenzo[a,d]cycloheptenone inhibitor-p38alpha MAP kinase complex in solution. *Angew Chem Int Ed Engl* **2012**, *51* (10), 2359-62.
45. Morris, G. M., et al., AutoDock4 and AutoDockTools4: Automated docking with selective receptor flexibility. *J Comput Chem* **2009**, *30* (16), 2785-91.
46. Trott, O.; Olson, A. J., AutoDock Vina: improving the speed and accuracy of docking with a new scoring function, efficient optimization, and multithreading. *J Comput Chem* **2010**, *31* (2), 455-61.
47. Pettersen, E. F., et al., UCSF Chimera--a visualization system for exploratory research and analysis. *J Comput Chem* **2004**, *25* (13), 1605-12.
48. Wang, J., et al., Automatic atom type and bond type perception in molecular mechanical calculations. *J Mol Graph Model* **2006**, *25* (2), 247-60.
49. Peti, W.; Page, R., Molecular basis of MAP kinase regulation. *Protein Sci* **2013**, *22* (12), 1698-710.